Physicochemical Characterization of Two Protic Hydroxyethylammonium Carboxylate Ionic Liquids in Water and Their Mixture

Augusto, Ferrari Felipe; Francisco, Malaret; Stephen, Eustace; Jason, Hallett; Luuk, Van Der Wielen; Geert-Jan, Witkamp; Bruno, Forte Marcus

DOI
10.1021/acs.jced.1c00687

Publication date
2022

Document Version
Final published version

Published in
Journal of Chemical and Engineering Data

Journal of Chemical&Engineering Data

pubs.acs.org/jced Article

Physicochemical Characterization of Two Protic Hydroxyethylammonium Carboxylate Ionic Liquids in Water and Their Mixture

Ferrari Felipe Augusto, Malaret Francisco, Eustace Stephen, Hallett Jason, van der Wielen Luuk, Witkamp Geert-Jan, and Forte Marcus Bruno*

Cite This: J. Chem. Eng. Data 2022, 67, 1309−1325 Read Online

ACCESS | Metrics & More | Article Recommendations | Supporting Information

ABSTRACT: A systematic study on the physicochemical properties of two protic ionic liquids (ILs) {2-hydroxyethylammonium acetate ([Mea][Ac]) and 2-hydroxyethylammonium hexanoate ([Mea][Hex])} and their mixtures with water was performed. The density and viscosity were assessed across the entire range of aqueous dilutions between 278 and 393 K. The conductivities, water activities, and surface tension of the binary systems in water were also assessed, and the influence of anions was evaluated. Differential scanning calorimetry (DSC), Fourier transform infrared (FTIR), and ^{1}H and ^{13}C nuclear magnetic resonance (NMR) techniques were used to study the systems at different IL compositions. The excess molar volumes (V^{E}) and thermal expansion coefficients were calculated, with negative values for V^{E} across the entire concentration range. Density data were fitted to a polynomial for density prediction, function of temperature, and concentration, with the average deviation percentage not exceeding 0.63%. The viscosities of the binary systems were studied considering six different models and were better predicted by the model of Herráez et al. at IL concentrations higher than 0.25 mole fraction. The systems containing $[Hex]^{-}$ exhibited higher water activities and lower conductivity and surface tension. All studied systems exhibited a glass transition event, which varied according to the IL composition. The FTIR and NMR analysis confirmed the distinct molecular arrangement of [Mea][Ac] and [Mea][Hex] systems.

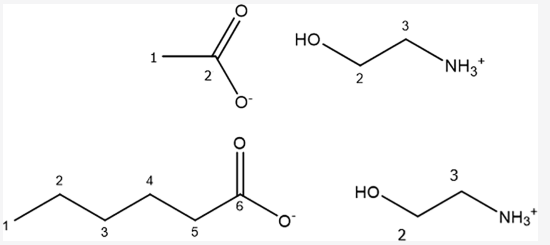

INTRODUCTION

Recently, much attention has been given to ionic liquids (ILs), whose structure can be designed based on process necessities and tuning properties such as viscosity, density, conductivity, and hydrogen bond potential. Therefore, physicochemical properties can be conveniently tuned to favor more efficient processes by carefully selecting the cation and the anion. The number of possible ILs is extremely large, which implies that there should be an optimum IL with the desired chemical and physical properties.[1]

ILs can be involved in different kinds of interactions, *e.g.*, H-bonding, Coulombic, van de Waals, solvophobic, and dipole−dipole.[2] Thereby, studies involving IL applications are found in a wide range of fields, from catalysis to solvent applications.[3,4] Protic ILs (PILs), characterized by a proton transfer between a cation and anion, are an attractive sort of IL for large-scale applications due to their lower cost, lower toxicity, and easier synthesis in comparison to aprotic ILs.[5,6] The fact that PILs contain proton donor and acceptor sites leads to an increased contribution of H-bonding to the cation−anion interaction, reducing the electrostatic network and conferring distinct bulk properties for this class of ILs.[2,7,8] The presence of hydroxyl groups in the cation, such as those found in ethanolamine, increases the heterogeneity from the bulk, hindering polar and apolar segregation.[2,9] Oxygen functionalized groups are also described to increase IL viscosity and promote a H-bonding network, more pronounced in groups with higher electron densities such as hydroxyl and ester groups.[2,9−11] The anions' alkyl chain has a direct impact on IL properties depending on its length.[12] Both an increase and a decrease in IL viscosity have been reported while increasing the anion alkyl chain.[11,13,14]

Among PILs, ammonium-based ILs, such as ethanolamine, have been reported as being an efficient class of solvents for agricultural residue valorization.[15−17] Agricultural residues are an essential source of raw material for bio-based and circular economy, and therefore, the efficient design of a process involving ethanolamine-based ILs is highly advantageous. The physicochemical properties, such as density and viscosity, of 2-hydroxyethylammonium acetate ([Mea][Ac]) were previously reported in the literature,[8,18,19] and it was found that even small variations in the IL's composition can impact the

Received: October 25, 2021
Accepted: April 22, 2022
Published: May 16, 2022

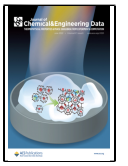

Table 1. List of Chemicals

component	CAS no.	linear formula	supplier	mass fraction	molecular weight	method of purity determination
acetic acid	64-19-7	CH_3CO_2H	Sigma Aldrich	≥0.997	60.05	gas chromatography
hexanoic acid	14-62-1	$CH_3(CH_2)_4CO_2H$	Sigma Aldrich	≥0.99	116.16	gas chromatography
ethanolamine (2-aminoethanol)	141-43-5	$NH_2CH_2CH_2OH$	Sigma Aldrich	≥0.99	61.08	gas chromatography
glycerol (propane-1,2,3-triol)	56-81-5	$HOCH_2CH(OH)CH_2OH$	Sigma Aldrich	≥0.995	92.09	gas chromatography
potassium chloride	7447-40-7	KCl	Sigma Aldrich	≥0.99	74.55	titration by $AgNO_3$
ultra-pure water	7732-18-5	H_2O	MilliQ Water	≥0.999	18.02	conductivity and resistivity
2-hydroxyethylammonium acetate	54300-24-2	$NH_3^+CH_2CH_2OH$ $CH_3CO_2^-$	this work	≥0.99	121.13	proton NMR
2-hydroxyethylammonium hexanoate		$NH_3^+CH_2CH_2OH$ $CH_3(CH_2)_4CO_2^-$	this work	≥0.99	177.24	proton NMR

properties of the final system. The presence of water in some potential areas of IL application is difficult to avoid. Moreover, water dilution can be used to decrease IL's viscosity and therefore improve mass transfer. Besides the cation−anion combination, mixtures of ILs can be used to fine-tune system properties for a more efficient process.[20−22] In a previous work, mixtures of [Mea][Ac] and 2-hydroxyethylammonium hexanoate ([Mea][Hex]) were efficiently applied to improve the solubilization of natural polymers and enhance cellulose enzymatic conversion.[22] The mixture of [Mea][Ac] and [Mea][Hex] was later studied during IL recovery from aqueous streams, where their distinct effect on the water freezing temperature was observed.[23]

The objective of this work is to study and report experimental measurements of density, viscosity, conductivity, surface tension, and water activity for [Mea][Ac], [Mea][Hex], and their aqueous solutions, exploring the influence of the mixtures in the physicochemical properties and molecular bulk characteristics. The temperature influence on density and viscosity was explored. Bulk property observations were linked to the molecular scale by means of differential scanning calorimetry (DSC), Fourier transform infrared (FTIR), and nuclear magnetic resonance (NMR) experiments.

MATERIAL AND METHODS

Synthesis and Sample Preparation. All the chemicals involved in the present work are presented in Table 1. Acetic acid (99.7%), hexanoic acid (99%), and ethanolamine (99%) were acquired from Sigma Aldrich. MilliQ water was used for dilution. 2-Hydroxyethylammonium acetate ([Mea][Ac]) and 2-hydroxyethylammonium hexanoate ([Mea][Hex]), depicted in Figure 1, were synthesized in 100 mL Schott flasks by a one-step, acid−base exothermic neutralization. First, ethanolamine was weighed into a flask. The flask was closed with a silicone septum and placed in a cold-water bath. An equimolar quantity of either acetic acid or hexanoic acid was slowly added through the septum using a syringe. The reaction was carried out overnight at room temperature under agitation. The formation of [Mea][Ac] or [Mea][Hex] was confirmed by proton nuclear magnetic resonance (^{1}H NMR); spectra are provided in the Supporting Information (SI); and the chemical shifts for the neat ILs, assigned in Figure 1, are as follows:

[Mea][Ac] ^{1}H NMR (δ ppm): Mea H-2 (3.15); Mea H-3 (3.87); Ac H-1 (2.01)/[Mea][Ac] ^{13}C NMR (δ ppm): Mea C-2 (41.07); Mea C-3 (57.7); Ac C-1 (23.66); Ac C-2 (178.15).

[Mea][Hex] ^{1}H NMR (δ ppm): Mea H-2 (3.15); Mea H-3 (3.89); Hex H-1 (2.26); Hex H-2 (1.68); Hex H-3,4 (1.44); Hex H-5 (1.03)/[Mea][Hex] ^{13}C NMR (δ ppm): Mea C-2 (41.24); Mea C-3 (57.71); Hex C-1 (13.3); Hex C-2 (22); Hex C-3 (25.63); Hex C-4 (31.38); Hex C-5 (37.4); Hex C-6 (180.35).

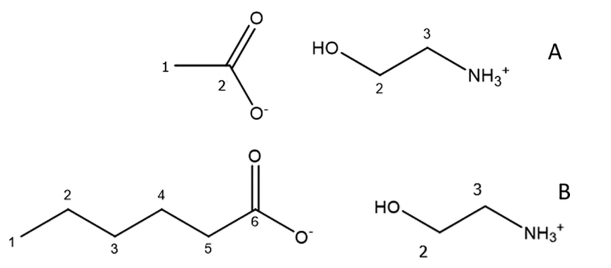

Figure 1. (A) [Mea][Ac] and (B) [Mea][Hex]. Numbers assign atoms for NMR spectra.

The water contents for [Mea][Ac] and [Mea][Hex] were 0.15 and 0.2% (w/w), respectively, assessed through Karl Fisher titration. For the mixture samples, either water or ILs were weighted with a precision of 1×10^{-4} g and then vigorously mixed for complete homogenization. Samples were sonicated for 2 h in sealed flasks at 45 °C and kept in a desiccator until analysis.

Volumetric Properties. Densities (ρ's) of pure ILs, mixtures, and aqueous solutions were measured in the range of 298.15 to 396.15 K at the atmosphere pressure by means of a vibrating tube densitometer (DMA 5000M, Anton Paar, Austria) with a precision of 1.0×10^{-6} g cm^{-3} and 1.0×10^{-3} °C. The relative uncertainty u_r (ρ) of 0.0019, 0.0028, and 0.0025 refers to the measurements of [Mea][Ac], [Mea][Hea], and the mixture, respectively, assuming that the difference between the density of the sample and impurities is 10%.[24] The instrument was calibrated before each experimental run using dry air and water. At the end of each run, the density of MilliQ water was acquired for consistency. Aqueous samples were measured in triplicate and five times for the density of dry ILs.

The molar volume (V_m) was calculated according to eq 1, and the excess molar volumes (V^E) was calculated using eq 2

$$V_m = \frac{(x_1M_1 + x_2M_2)}{\rho_{mix}} \quad (1)$$

https://doi.org/10.1021/acs.jced.1c00687
J. Chem. Eng. Data 2022, 67, 1309−1325

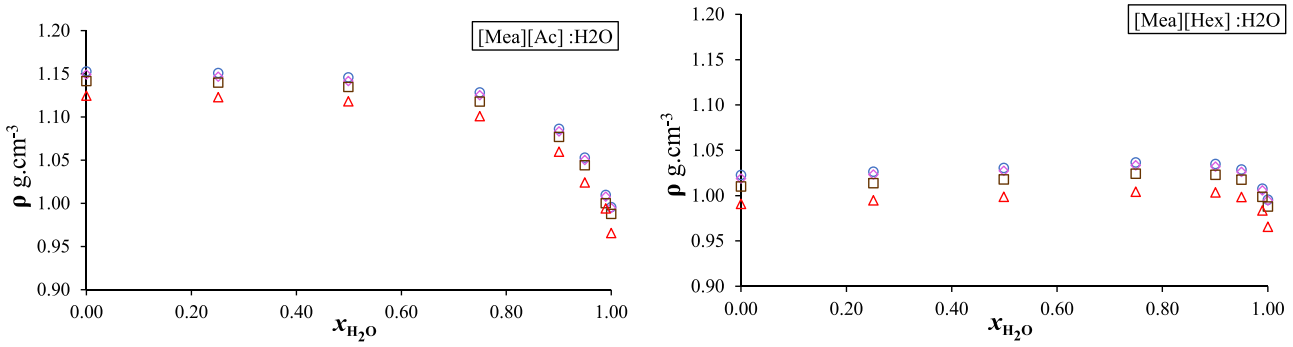

Figure 2. Density versus water mole fraction at different temperatures: 298.15 K (blue circles), 303.15 K (blue diamonds), 318.15 K (brown squares), and 348.15 K (red triangles). Error bars not shown but provided in Table 2.

$$V^E = V_m - \frac{x_1 M_1}{\rho_1} - \frac{x_2 M_2}{\rho_2} \quad (2)$$

where x_i denotes for the mole fraction of the component, M_i is the molar mass, and ρ_i is the density. The correction of density due to viscosity is done automatically by the equipment.

The thermal expansion coefficient (α_p) indicates the volume dependence on temperature and was calculated according to eq 3.

$$\alpha_p = \frac{1}{V}\left(\frac{\partial V}{\partial T}\right)_p = -\left(\frac{\partial \ln \rho}{\partial T}\right)_p \quad (3)$$

The molecular volume for a single IL pair was calculated using eq 4, where N_a is the Avogadro constant ($6.02214076 \times 10^{23}$ mol^{-1}) and M_{IL} is the molar mass.

$$V_m^f = \frac{M_{IL}}{N_a \cdot \rho_{IL}} \cdot \frac{10^{21}\ \text{nm}^3}{\text{cm}^3} = 1.6605 \cdot 10^{-3} \frac{\text{Mw}_{IL}}{\rho_{IL}} \quad (4)$$

Viscosity. Viscosities (η's) of pure IL, mixtures, and aqueous solutions were measured in the range of 298.15 to 323.15 K at the atmosphere pressure by means of a rolling ball tube (Lovis 2000M/ME, Anton Paar, Austria) with an accuracy of 0.5% and 2.0×10^{-2} °C. The instrument was calibrated before each experimental run with MilliQ water and standard oil provided by the manufacturer. At the end of each run, the viscosity of MilliQ water and glycerol was acquired for consistency purposes. For samples without water addition at ambient temperature (298.15 K), viscosities were measured using a cone-plate model rheometer (AR1500ex, TA Instruments, USA) due to their high viscosities. The shear rate used was 1 s^{-1}, from 0 to 300, with a cone diameter of 20 mm at 298.15 K. Aqueous samples were measured in triplicate and five times for the dry ILs.

Conductivity. Conductivities were acquired through electrical potential (DC) measurements by means of a self-made platinum probe coupled to a multiparameter analyzer (CONSORT C832, Belgium) at ambient temperature (≈293 K) in a climatized room. The conductivity was calculated through a KCl calibration curve. The probe was exhaustively rinsed, until the same conductivity of pure water was observed, and dried between measurements. The setup was verified against ultrapure water and a standard KCl solution (0.1 M) with a relative uncertainty u_r (σ) = 0.05.

Water Activity. Water activity (a_w) was measured through vapor sorption analysis using a Q5000 SA (TA Instruments, USA) with a weight sensitivity of <0.1 μg and accuracy of 0.01%, isothermal stability of ±0.1 °C, and humidity accuracy in the humidity chamber of ±1% relative humidity (RH). Aqueous IL samples were weighted in platinum pans; mass variations were acquired as the humidity inside the chamber was changed until a constant weight was achieved. Then, the humidity was decreased and the mass was recorded after equilibrium, and the process was repeated. After the desorption run, the humidity in the chamber was increased at a constant level, and the mass variation due to the water adsorption was recorded. The a_w was assumed to be RH/100 at the equilibrium. Measurements were performed in triplicate.

Surface Tension. Surface tensions were measured against air at room temperature (≈293 K) by means of the pendant drop method using DSA25S Krüss (Germany). Samples were placed in a syringe, and the drop generated out of the cannula was photographed. From the digital shape of the drop, surface tension was calculated by solving Laplace's equation for the curvature of the interface exposed to a gravitational field. Standard uncertainty $u(\sigma)$ was ±1.4−2.2 mN m^{-1}.

Differential Scanning Calorimetry (DSC). The glass transition (T_g) of the ILs was determined using a calorimeter (DSC8500 PerkinElmer, USA) in a cooling−heating cycle at 10 K min^{-1}. The ILs were first heated from 163.15 to 396.15 K to remove the previous thermal history. Then the sample was cooled down to 153.15 K, kept for 20 min, and heated again to 323.15 K.

FTIR

A PerkinElmer Spectrum 100 FT-IR spectrometer with a diamond germanium ATR single reflection crystal was used. The spectra were recorded between 500 and 4000 cm^{-1} with a resolution of 2 cm^{-1}, and each sample was scanned 16 times.

NMR

All measurements were performed at 298.15 K in a 5 mm borosilicate NMR tube containing a sealed 3 mm capillary containing deuterated benzene used for locking and shimming. All spectra were referenced to C_6D_5H at 7.15 ppm in the proton spectra and 127.00 ppm for ^{13}C for C_6D_6. The proton spectra were recorded using eight scans, a relaxation delay of 1.0 s, and an acquisition time of 2.56 s at a 45° hard pulse width at 399.67 MHz. The carbon spectra were recorded using 256 scans, a relaxation delay of 1.0 s, and an acquisition time of 1.31 s at a 45° hard pulse width at 100.51 MHz. The spectra were processed using MestReNova version 12.01 with no apodization applied. All measurements were performed using an Agilent 400MR fitted with a OneNMR probe.

https://doi.org/10.1021/acs.jced.1c00687
J. Chem. Eng. Data 2022, 67, 1309−1325

RESULTS

The results are elaborated in respect to the following systems:

i. Pure ILs: [Mea][Ac] and [Mea][Hex]
ii. Binary systems: aqueous solutions of [Mea][Ac], aqueous solutions of [Mea][Hex], and mixture of [Mea][Ac] and [Mea][Hex]
iii. Tertiary systems: aqueous solutions of [Mea][Ac] and [Mea][Hex] mixtures.

The mixture of the neat ILs favors a bulkier molecular packing, as suggested by the glass transition temperature and the rheological stability upon temperature increase from the Vogel−Tammann−Fulcher equation. Density varies following ideality, while viscosity exhibits a non-ideal behavior. Water tends to bind preferentially in the charged molecular groups, leading to non-ideal mixtures for density and viscosity. Results suggest [Mea][Hex] aggregation in the diluted regions, as suggested by the Walden plot, FTIR, and NMR data. The longer alkyl chain of $[Hex]^-$ leads to relevant hydrophobicity as observed by surface tension and water activity data. FTIR and NMR data suggest different molecular structure and water influence between [Mea][[Ac] and [Mea][Hex] systems.

Volumetric Properties. The volumetric properties of [Mea][Ac] and [Mea][Hex] systems as a function of temperature and water mole fraction are depicted in Figures 2−6. The data for the binary systems are summarized in Table 2, and those for the tertiary systems are in Table S1 of the Supporting Information (SI).

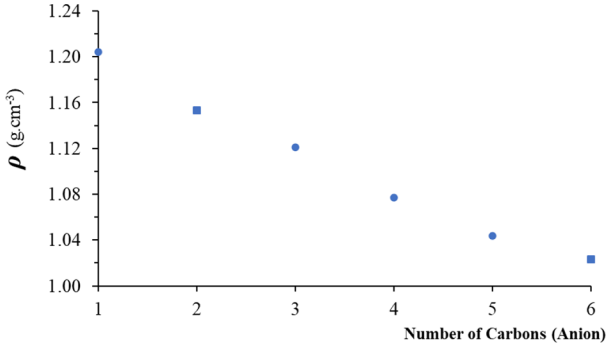

Figure 3. Density and viscosity of ILs based on 2-hydroxyethylammonium cation as a function of anion alkyl chain length. Data from Hosseini (2018): C_1, Sarabando (2018): C3, Yunus (2019): C_4, Rocha Pinto (2015): C_5, and this work: C_2 and C_6.

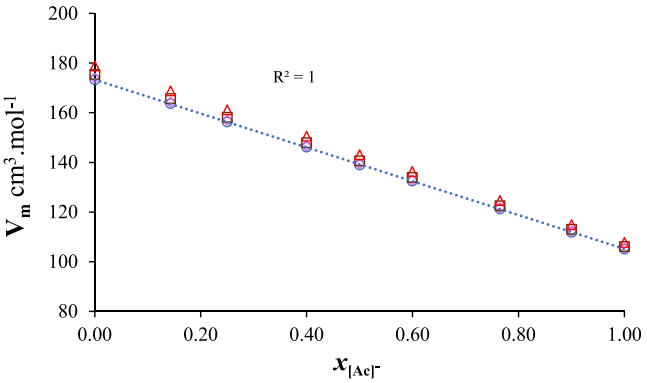

Figure 5. Molar volume of the [Mea][Hex]:[Mea][Ac] mixture as a function of mole fraction at different temperatures: 298.15 K (blue circles), 303.15 K (blue diamonds), 318.15 K (brown squares), and 348.15 K (red triangles). Error bars not shown but provided in the SI. Mole fractions do not consider the trace water content of ILs (<0.01%).

An increase in the anion's alkyl chain length leads to a lower density of [Mea][Hex] as expected, which might be attributed to the bulkier chains increasing steric hindrance. Water has a minimum effect on the density of [Mea][Ac] up to 0.5 mole fraction, as shown in Figure 2, with increased influence on this physical property at higher concentrations, a fact that was also observed by Alvarez et al.[18] Water content affects [Mea][Hex] distinctly; the density slightly increases with increasing water up to a maximum at 0.9 mole fraction and then decreases toward the density of pure water. This trend is in agreement with a previous study for other ammonium alkanoate based ILs.[25]

In Figure 3, the density of different ILs based on 2-hydroxyethylammonium cation is depicted. Literature data for formate, lactate, butyrate, and pentanoate were used and compared with the values found in the present study for acetate and hexanoate to assess the influence of increasing the anion's alkyl chain.[26−29] It is possible to observe a linear (r^2 = 0.9861) decrease in the density as the number of carbons increases. As further discussed in the Surface Tension section, it is assumed that the anion alkyl chains are located toward the region exposed to the air, or void. Assuming this molecular organization, the increase in the carbon chain length hinders the entanglement of the alkyl chains, favoring the formation of

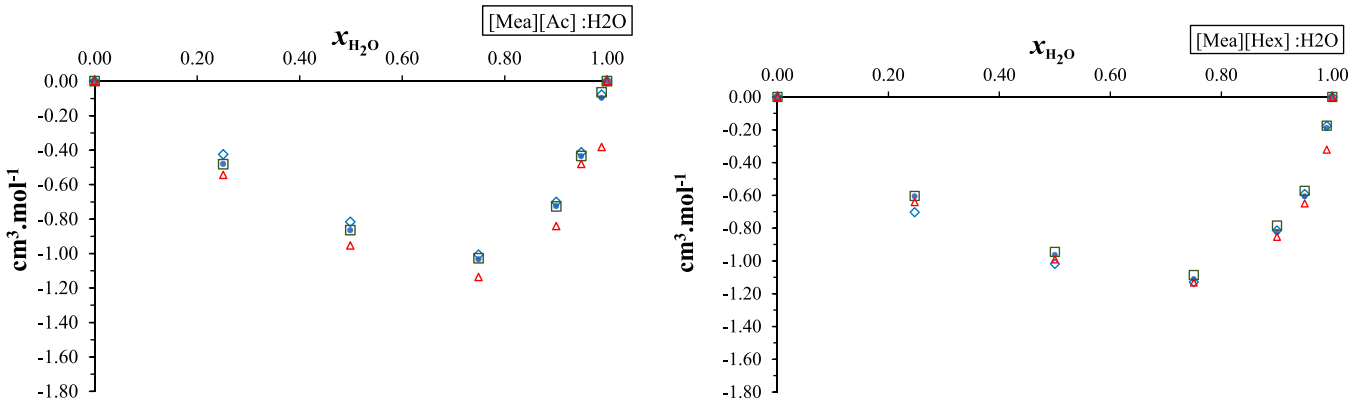

Figure 4. Excess molar volumes as a function of water mole fraction at different temperatures: 298.15 K (blue circles), 303.15 K (blue diamonds), 318.15 K (brown squares), 348.15 K (red triangles), and 363.15 K (x). Error bars not shown but provided in the SI.

https://doi.org/10.1021/acs.jced.1c00687
J. Chem. Eng. Data 2022, 67, 1309−1325

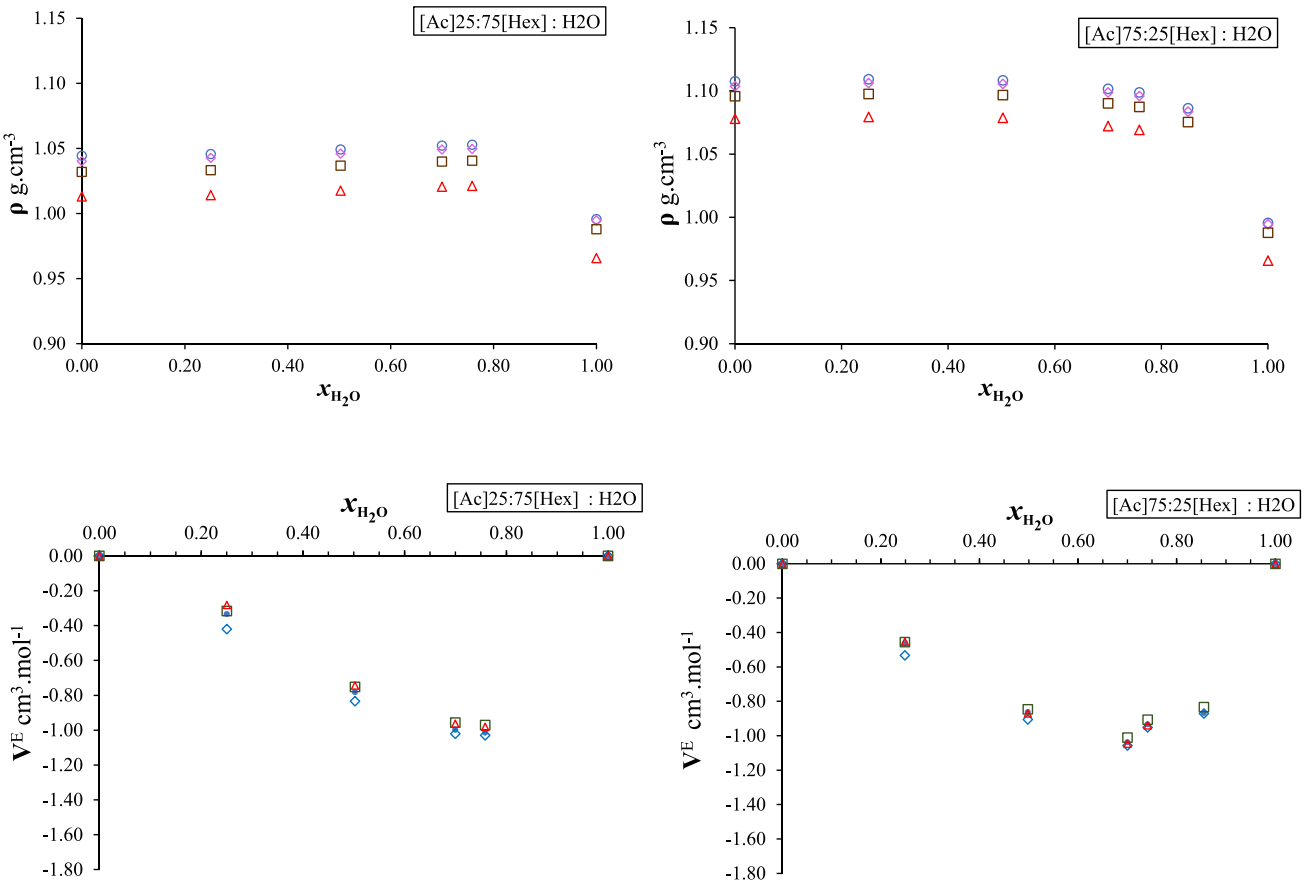

Figure 6. Density (ρ: top) and excess molar volume (V^E: bottom) of [Mea][Hex]:[Mea][Ac] mixtures as a function of water mole fraction for two IL compositions at different temperatures: 298.15 K (blue circles), 303.15 K (blue diamonds), 318.15 K (brown squares), and 348.15 K (red triangles). Error bars not shown but provided in the SI.

free space within the bulk, which might explain the progressive decrease in density.

Excess molar volumes (V^E's) were considered to assess the influence of mixtures on the volumetric profile. V^E was calculated using eq 2. For both ILs, the V^E's are negative across the entire range of aqueous dilutions, with a minimum at a water mole fraction near 0.75. The negative values indicate that the attractive forces between the different molecules are greater than those from the same molecules in the neat solvent. The longer alkyl chain from [Mea][Hex] had no evident effect on V^E, which is reasonable since water tends to bind to the H-bonding sites, i.e., the COO^- (anion) and NH_3^+ and OH (cation).[30,31]

The anhydrous mixtures of [Mea][Ac] and [Mea][Hex] exhibited a linear (r^2 = 1) change in the molar volume following the variation in the molar composition, suggesting mixing ideality for this system, as depicted in Figure 5. The thermal expansion (α_p) of [Mea][Ac] was found to be inferior to that observed from [Mea][Hex], 0.5×10^{-3} and 0.6×10^{-3} K^{-1}, respectively. For the mixtures, the calculated α_p changed proportionally to the increase of one of the components, i.e., $[Ac]^-$ and $[Hex]^-$, as shown in Figure S2 (SI).

Two distinct molar compositions were selected to assess the influence of water on the mixtures, namely, 0.25:0.75 and 0.75:0.25 [Mea][Ac]:[Mea][Hex] mole fraction, respectively. Density and V^E are depicted in Figure 6; the complete data are available in the SI. As expected, the system richer in [Mea][Ac] exhibited a higher density. Similarly to the dilution of pure [Mea][Hex], the density of mixtures exhibited a slight increase as the water content increased, which persists at higher dilutions in the $[Hex]^-$ richer system (0.25:0.75). The V^E values for the mixtures are similar to those for the pure ILs, with the minimum for 0.25:0.75 composition moderately dislocated toward the IL-rich zone.

The calculated molecular volume for a single IL pair (eq 4) is 0.17 and 0.29 nm^3 for [Mea][Ac] and [Mea][Hex], respectively. These values were used to estimate the heat capacities using volume-based thermodynamics (VBT) correlation, eq 5,[32] which is believed to provide a result with a maximum mean absolute error of 24.5%. The calculated C_p values are 226 J mol^{-1} K^{-1} (1.87 J g^{-1} K^{-1}) and 343 J $mol^{-1}.K^{-1}$ (1.94 J g^{-1} K^{-1}) for [Mea][Ac] and [Mea][Hex], respectively.

$$C_p\ [\mathrm{J\ mol^{-1}\ K^{-1}}] = 1037 V_m^f\ [\mathrm{nm^3}] + 45 \quad (5)$$

Transport Properties. *Viscosity and Conductivity.* Generally, the high viscosity of ILs represents a major limitation to their use due to the poor heat and mass transfer and overall handling in process equipment. Therefore, the effects of temperature and water content on the viscosity of [Mea][Ac], [Mea][Hex], and their mixtures were assessed. Data for binary systems are provided in Table 2, and those for the tertiary systems are in the SI.

The characteristic of the anion has a clear influence on the viscosity of the resulting IL. Previous work has reported either an increase or a decrease in viscosity while increasing anion

https://doi.org/10.1021/acs.jced.1c00687
J. Chem. Eng. Data 2022, 67, 1309−1325

Table 2. Density (ρ = g cm^{-3}) and Viscosity (η = mPa S) of the Binary Systems as a Function of Molar Composition and Temperature (K) at Ambient Pressure (P = 81.5 kPa)

	[Mea][Ac] (x1) in H_20					[Mea][Hex] (x1) in H_20					[Mea][Ac] (x1) in [Mea][Hex]				
T (K)	x1	ρ	σ	σ	σ	x1	ρ	σ	σ	σ	x1	ρ	σ	σ	σ
298.15	0.0104	1.00974	0.00118			0.0100	1.00764	0.00026	1.35	0.12	0.1433[a]	1.03379	0.00034	1661.94	71.56
298.15	0.0503	1.05294	0.00118	2.08	0.05	0.0501	1.02886	0.00043	3.93	0.14	0.2500[a]	1.04440	0.00093	1710.19	72.20
298.15	0.0993	1.08647	0.00132	4.39	0.32	0.0998	1.03500	0.00001	12.14	0.46	0.4000[a]	1.05915	0.00003	1714.00	69.82
298.15	0.2506	1.12866	0.00028	27.23	0.36	0.2499	1.03652	0.00098	59.74	0.00	0.4999[a]	1.07336	0.00196	1999.31	73.26
298.15	0.5011	1.14590	0.00027	221.43	13.76	0.4999	1.03056	0.00098	280.26	14.23	0.5994[a]	1.08405	0.00032	2096.25	80.13
298.15	0.7489	1.15091	0.00022	872.99	90.30	0.7529	1.02648	0.00122	828.70	80.54	0.7651[a]	1.10767	0.00085	2193.25	70.90
298.15	0.9810[a]	1.15285	0.00015	2654.38	59.70	0.9715[a]	1.02276	0.00120	1590.31	50.44	0.9003[a]	1.13272	0.00250	2153.81	72.45
303.15	0.0104	1.00769	0.00115			0.0100	1.00580	0.00044			0.1433	1.03066	0.00034	1258.57	74.42
303.15	0.0503	1.05034	0.00140	1.90	0.11	0.0501	1.02619	0.00042	3.42	0.09	0.2500	1.04026	0.00060	1292.70	94.30
303.15	0.0993	1.08344	0.00207	3.78	0.27	0.0998	1.03208	0.00001	10.08	0.34	0.4000	1.05608	0.00003	1380.45	89.35
303.15	0.2506	1.12515	0.00152	21.92	0.25	0.2499	1.03351	0.00142	47.49	0.65	0.4999	1.06931	0.00241	1410.80	89.75
303.15	0.5011	1.14179	0.00110	138.94	12.73	0.4999	1.02744	0.00100	210.42	11.50	0.5994	1.08105	0.00009	1593.97	103.63
303.15	0.7489	1.14675	0.00117	598.33	42.40	0.7529	1.02334	0.00109	597.47	38.70	0.7651	1.10375	0.00099	1536.35	234.45
303.15	0.9810	1.14935	0.00112	1282.60	84.30	0.9715	1.01882	0.00119	1099.90	80.18	0.9003	1.12986	0.00001	1623.60	336.26
318.15	0.0104	1.00014	0.00109			0.0100	0.99869	0.00117			0.1433	1.02123	0.00035	476.60	28.57
318.15	0.0503	1.04412	0.00125	1.33	0.05	0.0501	1.01772	0.00039	2.30	0.06	0.2500	1.03193	0.00094	481.30	34.64
318.15	0.0993	1.07699	0.00129	2.54	0.17	0.0998	1.02304	0.00002	5.93	0.12	0.4000	1.04683	0.00003	504.07	33.34
318.15	0.2506	1.11798	0.00027	12.56	0.25	0.2499	1.02416	0.00099	25.80	0.21	0.4999	1.06118	0.00198	508.22	43.25
318.15	0.5011	1.13493	0.00024	70.40	3.38	0.4999	1.01795	0.00110	97.72	2.60	0.5994	1.07199	0.00001	559.39	35.75
318.15	0.7489	1.13979	0.00021	223.05	12.40	0.7529	1.01385	0.00099	249.08	11.22	0.7651	1.09587	0.00084	566.36	78.44
318.15	0.9810	1.14163	0.00013	606.16	115.07	0.9715	1.01010	0.00121	475.11	30.17	0.9003	1.12125	0.00002	621.52	46.07
323.15	0.0104	0.99562	0.00207			0.0100	0.99564	0.00168			0.1433	1.01806	0.00035	348.44	22.54
323.15	0.0503	1.04047	0.00107	1.27	0.00	0.0501	1.01475	0.00038	2.01	0.07	0.2500	1.02774	0.00060	332.77	0.00
323.15	0.0993	1.07354	0.00215	2.25	0.15	0.0998	1.01992	0.00002	5.14	0.10	0.4000	1.04372	0.00004	373.33	24.83
323.15	0.2506	1.11430	0.00158	10.46	0.28	0.2499	1.02096	0.00110	21.55	0.24	0.4999	1.05708	0.00243	353.86	6.83
323.15	0.5011	1.13099	0.00112	49.80	3.25	0.4999	1.01480	0.00132	77.82	3.40	0.5994	1.06895	0.00001	400.30	26.19
323.15	0.7489	1.13558	0.00119	155.38	10.07	0.7529	1.01066	0.00128	191.69	10.93	0.7651	1.09191	0.00100	393.72	52.16
323.15	0.9810	1.13810	0.00114	413.89	79.96	0.9715	1.00611	0.00120	354.74	25.79	0.9003	1.11836	0.00002	448.82	32.89
348.15	0.0104	0.99417	0.02923			0.0100	0.98353	0.00022			0.1433	1.00232	0.00350		
348.15	0.0503	1.02420	0.00300			0.0501	0.99853	0.00019			0.2500	1.01307	0.00110		
348.15	0.0993	1.05993	0.00158			0.0998	1.00348	0.00062			0.4000	1.02793	0.00004		
348.15	0.2506	1.10098	0.00026			0.2499	1.00436	0.00085			0.4999	1.04263	0.00201		
348.15	0.5011	1.11815	0.00028			0.4999	0.99863	0.00088			0.5994	1.05351	0.00001		
348.15	0.7489	1.12310	0.00022			0.7529	0.99475	0.00108			0.7651	1.07801	0.00097		
348.15	0.9810	1.12468	0.00024			0.9715	0.99100	0.00132			0.9003	1.10371	0.00004		
363.15	0.0104	0.88960	0.01460			0.0100	0.95815	0.00050			0.1433	0.99232	0.00036		
363.15	0.0503	1.00424	0.00372			0.0501	0.98800	0.00006			0.2500	1.00313	0.00109		
363.15	0.0993	1.04782	0.00231			0.0998	0.99288	0.00013			0.4000	1.01812	0.00004		
363.15	0.2506	1.09194	0.00026			0.2499	0.99390	0.00070			0.4999	1.03293	0.00202		
363.15	0.5011	1.10921	0.00028			0.4999	0.98835	0.00117			0.5994	1.04393	0.00001		
363.15	0.7489	1.11417	0.00023			0.7529	0.98455	0.00100			0.7651	1.06873	0.00103		

https://doi.org/10.1021/acs.jced.1c00687
J. Chem. Eng. Data 2022, 67, 1309−1325

Table 2. continued

	[Mea][Ac] (x1) in H_2O				[Mea][Hex] (x1) in H_2O				[Mea][Ac] (x1) in [Mea][Hex]			
T (K)	x1	ρ	σ	σ	x1	ρ	σ	σ	x1	ρ	σ	σ
363.15	0.9810	1.11584	0.00027		0.9715	0.98090	0.00133		0.9003	1.09462	0.00004	

[a]Data using a cone-plate rheometer; standard deviation (σ) units: g cm^{-3} for density and mPa s for viscosity; standard uncertainties are $u(T)$ = 0.02 K and $u(P)$ = 0.5 kPa. Relative standard uncertainties are $u_r(\rho)$ 0.0019, 0.0028, and 0.0025 for [Mea][Ac], [Mea][Hea], and the mixture, respectively; u_r (η) = 0.05.

alkyl chain length.[8,13,14,33] At 298 K (25 °C), [Mea][Ac] exhibits a higher viscosity than [Mea][Hex], 2.7 and 1.6 Pa·s, respectively. The difference is reduced remarkably when increasing temperature, 1.3 and 1.1 Pa·s for [Mea][Ac] and [Mea][Hex], respectively, at 303 K.

Water addition had a great impact in IL viscosity, as shown in Figure 7, as expected due to the significantly lower viscosity

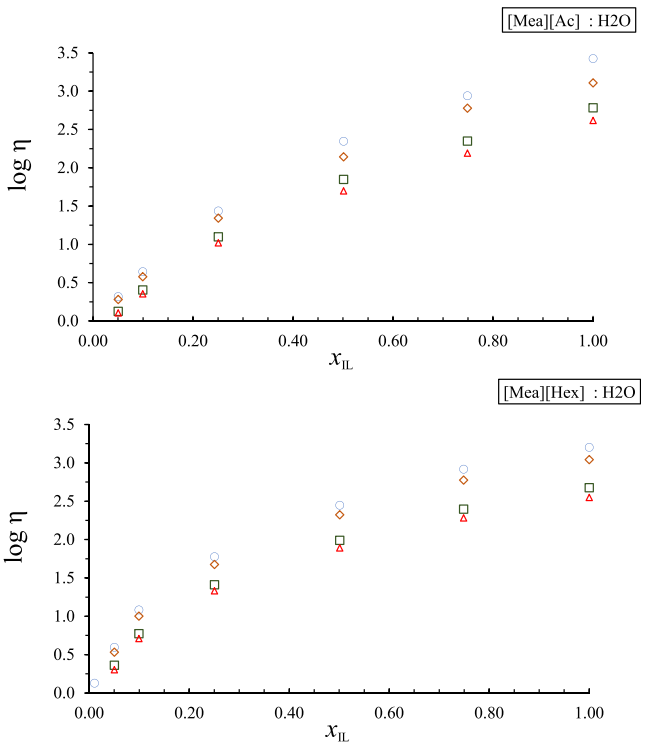

Figure 7. Log of viscosity as a function of IL mole fraction in water at different temperatures: 298.15 K (blue circles), 303.15 K (pink diamonds), 318.15 K (brown squares), and 323.15 K (red triangles). Mole fractions do not consider the trace water content of ILs (<0.01%).

of water compared to ILs. In the dilute region, at up to 0.25 IL mole fraction, aqueous [Mea][Hex] exhibited higher viscosities than aqueous [Mea][Ac], which is unexpected since the dry [Mea][Ac] has a higher viscosity.

The binary mixtures of the ILs were also assessed regarding viscosity, as shown in Figure 8. It is possible to observe the existence of two distinct regions defined by the molar composition. The viscosity remains stable despite the increase in [Mea][Ac] concentration up to 0.4 mole fraction. The same holds true for [Mea][Hex] up to 0.4 mole fraction. The equimolar composition assumes a transition point between the lower-viscosity region, [Mea][Hex]-richer region, and the higher-viscosity region, richer in [Mea][Ac]. The effect of temperature on viscosity was assessed with respect to the Vogel−Tammann−Fulcher (VTF)[34] equation according to eq 6.

$$\eta = \eta_0 \cdot e^{B/T-T_0} \tag{6}$$

where the angular coefficient corresponds to η_0, and T_0 and B are adjusted parameters. B is related to the pseudo-activation energy and can be taken as proportional to the Arrhenius activation energy (E_a),[35,36] giving a good indication of the rheological stability upon temperature increase. The fitting

https://doi.org/10.1021/acs.jced.1c00687
J. Chem. Eng. Data 2022, 67, 1309−1325

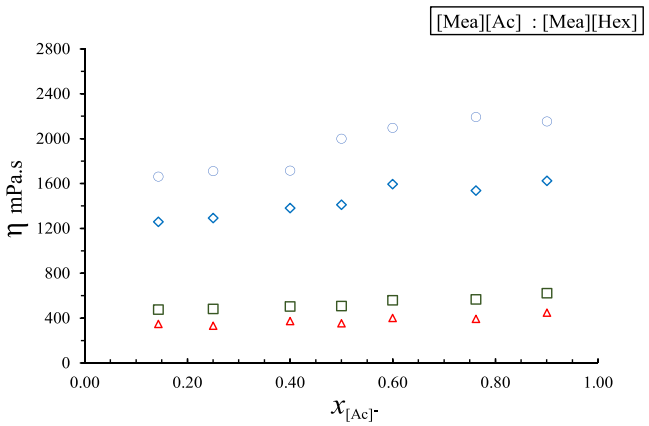

Figure 8. Viscosity of the [Mea][Hex]:[Mea][Ac] mixture in different ionic molar compositions at different temperatures: 298.15 K (blue circles), 303.15 K (pink diamonds), 318.15 K (brown squares), and 323.15 K (red triangles). Error bars not shown but provided in Table 2.

parameters, determination coefficient (r^2), and the average percentual deviation (APD) of the VTF equation are presented in Table 3. From the results in Table 2, it is possible to observe

Table 3. Fitting Parameters for the Vogel−Tammann−Fulcher (VTF) Correlation of Viscosity as a Function of the Temperature

mixtures	η_0 (mPa s)	T_0 (K)	B	r^2	APD[a] (%)
[Mea][Ac]	198.68	284.75	35.54	0.99878	6.3
[Mea][Hex]	195.03	249.535	205.26	0.99935	2.9
[Mea][Ac] 0.25:0.75 [Mea][Hex]	196.75	214.43	549.01	0.99547	18.7
[Mea][Ac] 0.50:0.50 [Mea][Hex]	203.03	203.34	746.35	0.99883	4.0
[Mea][Ac] 0.75:0.25 [Mea][Hex]	205.35	200.6	782.71	0.99922	3.3

[a] $(100/n)\cdot\sum[(\eta_{pred.} - \eta_{exp.})/\eta_{exp.}]$.

that [Mea][Ac] has a lower B than that obtained for [Mea][Hex], 35.24 and 205.26, respectively, and consequently, the viscosity of [Mea][Ac] is affected by temperature to a greater extent, in accordance with the experimental results. All IL mixtures exhibited B values higher than those observed for the pure ILs, suggesting that the viscosity of mixtures is less affected by temperature changes.

There are various equations to estimate the viscosity of mixtures in terms of pure component data. They may differ in whether they use adjustable parameters or not. Both types of equations were used to fit the experimental data to assess the best model to estimate the viscosity of [Mea][Ac]/[Mea][Hex]/water mixtures. Those without adjustable parameters include the Arrhenius mixing law for viscosity, given in eq 7.[37] Kendall and Monroe proposed eq 8, from which the mixture viscosity is calculated from the cubic-root average of the component viscosities.[38] Frenkel[39] considered Eyring's model[40] to take into consideration the interaction between components in a nonideal binary mixture, as demonstrated in eq 9, where η_{12} is a constant attributed to the pair interaction and is calculated according to eq 10.[41] Further approaches we assessed make use of adjustable parameters to account for nonidealities. Grunber and Nissan[37] correlated the natural logarithm of pure components' viscosities to that from the resulting mixture, including a so-called "characteristic constant of the system" (d_{12}, eq 11). Katti and Chaudhri[42] considered the volume of each component when correlating them to the viscosity of the resulting mixture. In this work, we substituted the component volume (V) by the inverse of density ($1/\rho$) to account for the volumetric characteristic of each component (eq 12). Herráez et al.[43] considered the Redlich−Kister polynomial, widely used for calculations of excess properties, to propose a model with the adjustable parameter B_0 (eq 13). APD calculated according to eq Sq.3 and the fitting parameters, when applicable, are summarized in Table 4. It was found that there is no unanimous model for best predicting the resulting viscosity for the studied systems. In general, the models had smaller deviations for the viscosities of the mixtures between [Mea][Ac] and [Mea][Hex], while larger deviations were found for the aqueous mixture predictions. The smallest deviations for the [Mea][Ac]/[Mea]Hex] mixture was achieved using the Katti−Chaudhri model, while the best choice for the aqueous system was found to be the Herráez model at IL mole fractions higher than 0.25. For dilute systems, under 0.25 mole fraction, deviations were not smaller than 20%.

$$\ln(\eta_{mix}) = x_1\cdot\ln(\eta_1) + x_2\cdot\ln(\eta_2) \quad (7)$$

$$\eta_{mix} = (x_1\eta_1^{1/3} + x_2\eta_2^{1/3})^3 \quad (8)$$

$$\ln(\eta_{mix}) = x_1^2\cdot\ln(\eta_1) + x_2^2\cdot\ln(\eta_2) + 2x_1x_2\ln(\eta_{12}) \quad (9)$$

$$\eta_{12} = 0.5\eta_1 + 0.5\eta_2 \quad (10)$$

$$\ln(\eta_{mix}) = x_1\cdot\ln(\eta_1) + x_2\cdot\ln(\eta_2) + x_1x_2d_{12} \quad (11)$$

$$\ln\left(\eta_{mix}\cdot\frac{1}{\rho}\right) = x_1\cdot\ln\left(\eta_1\frac{1}{\rho_1}\right) + x_2\cdot\ln\left(\eta_2\frac{1}{\rho_2}\right) + x_1x_2\left(\frac{W}{RT}\right) \quad (12)$$

$$\eta_{mix} = \eta_1 + (\eta_2 - \eta_1)\cdot x_2^{B_0} \quad (13)$$

Table 4. Average Deviation Percentage and Fitting Parameters for the Different Models Considered for the Prediction of Resulting Viscosity for IL Solutions and Mixture[a]

	Arrhenius mixing	Kendall−Monroe	Frenkel−Eyrin	Grunber and Nissan		Katti−Chaudhri		Herráez *et al.*	
	ADP (%)	ADP (%)	ADP (%)	d_{12}	ADP (%)	W/RT	ADP (%)	B_0	ADP (%)
[Mea][Ac] and H_2O	53.0	92.2	17.9	6.3021	16.6	5.9638	14.3	3.6905	29.7
[Mea][Hex] and H_2O	63.8	14.7	38.9	9.7184	44.9	9.5744	43.6	2.3484	18.7
[Mea][Ac] and [Mea][Hex]	7.6	8.3	19.4	−0.3157	92.5	−0.2615	5.1	1.8756	5.8

[a] ADP = $(100/n)\cdot\sum[(\eta_{pred.} - \eta_{exp.})/\eta_{exp.}]$.

https://doi.org/10.1021/acs.jced.1c00687
J. Chem. Eng. Data 2022, 67, 1309−1325

Conductivity data, important for electrochemical applications, can provide an insight to the mass transfer/diffusivity processes of organic electrolytes in water.[44] Conductivity data were acquired at room temperature (20−23 °C) from aqueous solutions of [Mea][Ac], [Mea][Hex], and their combination. In Figure 9, the conductivity is plotted versus solution molality.

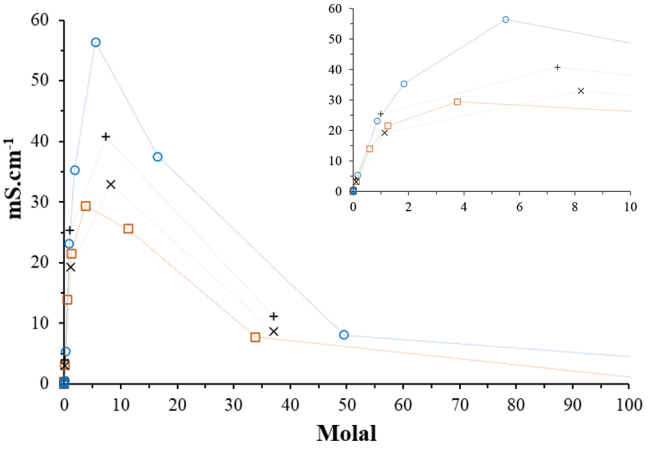

Figure 9. Conductivity as a function of IL molality: (blue circles) [Mea][Ac], (red squares) [Mea][Hex], (+) [Mea][Ac] 0.25:0.75 [Mea][Hex], and (x) [Mea][Ac] 0.75:0.25 [Mea][Hex]. Lines plotted for guidance. Error bars not shown but provided in the SI.

[Mea][Ac] exhibited the highest values among the assessed ionic systems. The conductivity increased at a higher rate up to 2 *m*, reaching a maximum around 5 *m*. The region of 5 *m* is reported as the critical point where the ionic species form ion pairs in [Mea][Ac], which corresponds to the maximum in conductivity observed. The remaining systems follow a similar trend to that described for [Mea][Ac], with the maximum point of [Mea][Hex] dislocated to more dilute regions though. Interestingly, the mixture with a higher mole fraction of [Hex] (0.25:0.75) presented a higher conductivity than that observed in the [Ac]-rich mixture (0.75:0.25), which might be attributed to the lower viscosity of the [Hex]-richer mixture. For this class of ILs, the proton conduction effect (Grotthuss mechanism) cannot be neglected as an influencing factor for conductivity,[45] further addressed in the FTIR section, which might explain the higher viscosity of [Mea][Ac] near the concentration of ion pairing reported in the literature.

Walden plots have been widely applied to evaluate the interplay between IL viscosity and conductivity at the same temperature. Generally, ILs can be classified as good, poor, and nonionic depending on their position on the chart, presenting poor ionicity as they move right to the bisectrix and reference line.[46] The characterization of the studied ILs with respect to the Walden plot is depicted in Figure 10. The ionic systems are distant to the reference line in accordance with their reported conductivities. [Mea][Ac] is the closest system in relationship to the reference line, which is expected due to its higher conductivity. [Mea][Hex] samples exhibit a clear nonlinear profile, not as evident in [Mea][Ac], which might suggest molecular aggregation, negatively affecting the conductivity, in addition to viscosity influence. Walden plots are also used to investigate the ionicity of protic ILs due to proton transfer from the acid to base[47] since poor proton transfer would lead to lower conductivity and, consequently, a farther position from the reference line. However, both [Mea][Ac] and

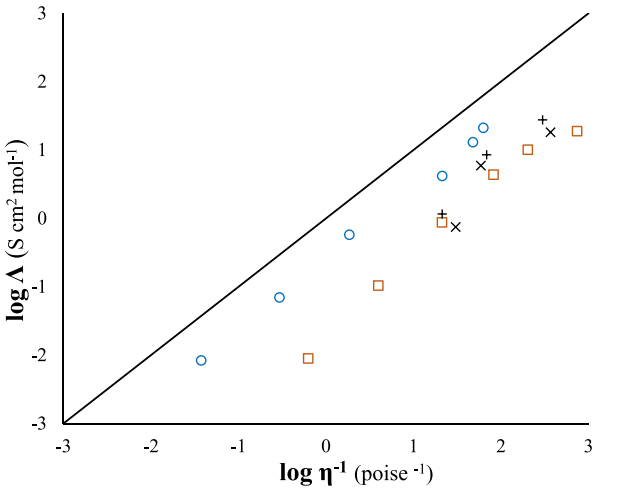

Figure 10. Walden plot for (blue circles) [Mea][Ac], (red squares) [Mea][Hex], (+) [Mea][Ac] 0.25:0.75 [Mea][Hex], and (x) [Mea][Ac] 0.75:0.25 [Mea][Hex].

[Mea][Hex] spectroscopic data suggest a good proton transfer; therefore, the deviation might arise for the high viscosity of these systems.

Differential Scanning Calorimetry (DSC). Samples of the pure ILs and their mixtures were submitted to DSC analysis to assess their thermal profile. The DSC thermograms and data are available in the SI. Pure [Mea][Hex] was the only one to exhibit a crystallization peak at 245.15 K (−28 °C). All samples presented well-defined glass transition temperatures (T_g's). T_g gives an indication about the cohesiveness of the sample's molecules. The less cohesive the molecules are, the lower the T_g is.[47] In ILs, the cohesive energy is mainly attributed to Coulombic and H-bonding interactions.[8,48] In Figure 11, T_g is plotted against the mole fraction of [Mea][Ac]

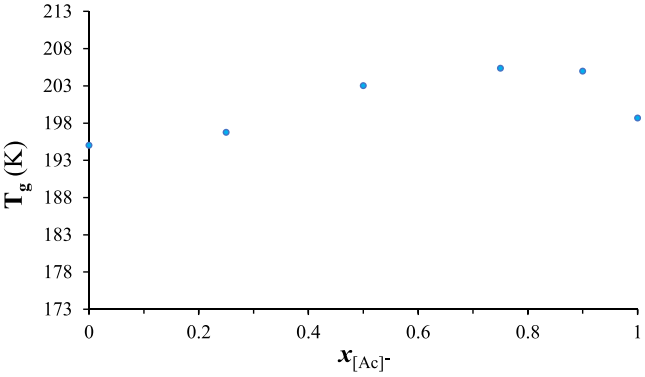

Figure 11. T_g values for [Mea][Ac]:[Mea][Hex] mixtures as a function of the [Mea][Ac] mole fraction.

in the ionic mixture. [Mea][Ac] has a marginally higher T_g than that observed for $[Hex]^-$, 198.68 K (−74.47 °C) and 195.03 K (−78.12 °C), respectively. Among the mixtures, the composition of 0.75 [Mea][Ac] presented the highest T_g, suggesting a higher molecular cohesiveness at this point, which agrees with the thermal sensibility data assessed through the VTF equation for viscosity dependence on temperature.

Glass-forming fluids can be classified as fragile or strong based on how sensitive to temperature their viscosities are.[47,49] The T_g-scaled Arrhenius plot, as depicted in Figure S4,

https://doi.org/10.1021/acs.jced.1c00687
J. Chem. Eng. Data 2022, 67, 1309−1325

Table 5. Water Activity (a_w) at Different IL Concentrations Expressed in Mass Fraction (IL %w) and Molal (mol kg^{-1} H_2O) at 298.15 K (25 °C) and at Ambient Pressure (P = 81.5 kPa)

[Mea][Ac]				[Mea][Hex]				[Mea][Ac] 0.5:0.5 [Mea][Hex]			
IL %w ± σ		molal[a]	a_w	IL %w ± σ		molal[a]	a_w	IL %w ± σ		molal[a]	a_w
93.0	0.5	219.4	0.11	86.8	0.6	74.2	0.35	86.3	0.8	84.4	0.35
79.0	0.2	62.1	0.35	74.1	0.7	32.3	0.65	68.3	0.7	28.9	0.65
56.7	0.2	21.6	0.65	69.0	0.3	25.1	0.73	61.4	0.3	21.3	0.73
49.4	0.3	16.1	0.73	58.6	0.7	16.0	0.84	47.9	0.8	12.3	0.84
37.0	0.2	9.7	0.84	30.1	0.2	4.9	0.95	21.3	0.3	3.6	0.95
17.0	0.8	3.4	0.95	15.4	0.6	2.1	0.98	11.0	0.7	1.7	0.98
8.0	0.5	1.4	0.98								

[a]Molalities assume complete ion dissociation in water. Standard uncertainty $u(T)$ = ±0.01 K, $u(P)$ = ±0.05 kPa, and $u(a_w)$ = ±0.2.

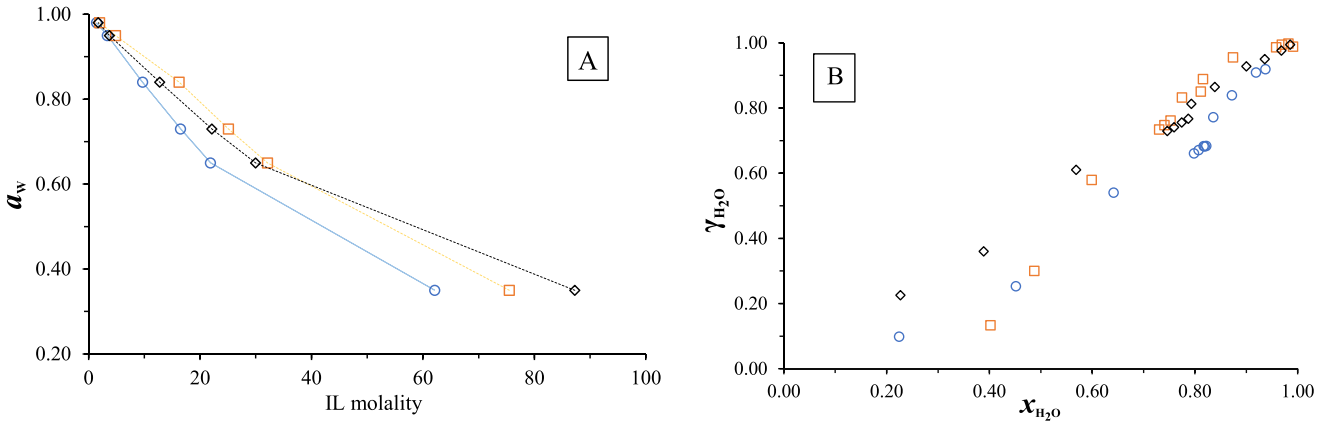

Figure 12. Water isotherm equilibrium in the different systems, where "A" depicts the water activity (a_W) as a function of IL molality and "B" the water activity coefficient (γ_{H2O}) as a function of water mol fraction (x_{H2O}): (blue circles) [Mea][Ac], (red squares) [Mea][Hex], and (black diamonds) equimolar [Mea][Ac]:[Mea][Hex]. Lines plotted for guidance purposes.

correlates the log η (Pa s) against T_g/T. The studied ILs, whether the pure ILs or their combination, occupy the same spot on the chart. Moreover, the similar activation energy observed during the viscosity assessment suggests that the higher T_g observed for the mixtures might be related to a more effective molecular packing and not additional chemical bonding. Solutions at water compositions of 0.75 mole fraction were used to assess the influence of water presence on T_g for the pure ILs and also for the mixture at 0.75 [Mea][Ac]. Water strongly interacts with the ions, hindering cation−anion interaction, decreasing overall cohesiveness, and thus lowering the T_g to 177 K (−96.15 °C) for the pure ILs and to 178 K (−95.15) for the mixture at 0.75.

Water Activity. Water activity (a_w) expresses the ratio between the partial vapor pressure of water in a substance and the standard vapor pressure of pure water, in other words, how easy the water content may be utilized or separated. As expected, no hysteresis effects were observed during water adsorption and desorption experiments, as shown in Figure S5. Nevertheless, the values for a_w, shown in Table 5, are related to the adsorption experiments where longer times were given to equilibrate. The IL concentrations resulted from the equilibrium of water between the sample and chamber humidity. In Figure 12, a_w is depicted as a function of IL concentration (A), and the water activity coefficient (γ_{H2O}) is shown as a function of the water mass fraction (B) for both ILs. An equimolar composition of [Mea][Ac] and [Mea][Hex] was also considered in others to assess the effect of having different anion chain lengths in mixtures. All systems have similar values for a_w in the ionic and water-rich regions; distinct profiles are more evident after 5 m. The longer alkyl chain from $[Hex]^-$ leads to larger hydrophobic regions, which in turn increase a_w. Similar trends were observed for the a_w calculated from the freezing point depression of IL−water mixtures by Ferrari et al.[23] The a_w profile from the IL mixture takes place in between those from the pure components; however, it exhibits a higher a_w in the region of lower water concentration.

Surface Tension. The measured surface tension for the pure ILs and for their mixtures while anhydrous or in aqueous solutions is available in Table S6 from SI. The molecular arrangement has a direct effect on surface tension. For these ILs, it is considered that the charged group, e.g., NH_3^+ and COO^-, will be located toward the bulk of the liquid, while the alkyl chains are exposed towards the air, or void.[19,47] The higher surface of the carbonic chain will decrease the surface tension, while the higher cohesiveness of the liquid due to H-bonding and Coulombic interaction will increase this property. [Mea]Hex] has a lower surface tension than [Mea][Ac], as expected. Although both ILs act decreasing water surface tension, [Mea][Hex] shows a better aptitude as a surfactant, as depicted in Figure 13.

The presence of $[Hex]^-$, concentration independent within the studied range, in the binary and tertiary systems confers the same surface tension of that from the pure [Mea][Hex], supporting the assumption of alkyl chains being located toward the interface. The mixture of [Mea][Ac] and [Mea][Hex] acts predominantly on the molecular arrangement of the alkyl chains. The fact that the surface tension of the aqueous systems is the same as that observed for the pure ILs suggests

https://doi.org/10.1021/acs.jced.1c00687
J. Chem. Eng. Data 2022, 67, 1309−1325

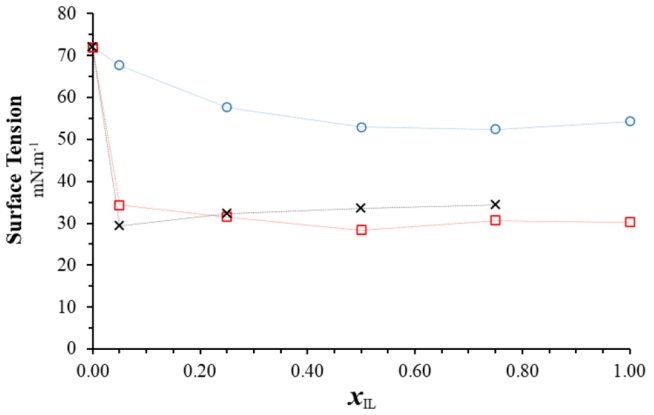

Figure 13. Surface tension as a function of IL mole fraction: (blue circles) [Mea][Ac], (red squares) [Mea][Hex], and (x) [Mea][Ac] 0.75:0.25 [Mea][Hex]. Lines used as guidance. Mole fractions do not consider the trace water content of ILs (<0.01%)

that the H-bonding is the major factor responsible for fluid cohesiveness and, consequently, the major force against surface expansion in these ILs.

Infrared. The ILs used in this study are completely miscible with water. To investigate the interactions between these ILs and water, the FTIR spectra were recorded as a function of water concentration for binary and tertiary mixtures (Figure 13). To the best of our knowledge, the FTIR spectra for these systems have not been previously reported; therefore, the spectral assignment is based on previous work involving the different moieties in these systems. The strong C═O stretching signal at 1707 cm^{-1} in the acetic acid and hexanoic acid FTIR spectra cannot be seen in any of the spectrum shown in Figure 14, suggesting a complete proton transfer from the acid to the amine. However, it is known that protic ionic liquids can form complex equilibria between the charged ions and the neutral species, especially when the difference in $\Delta pK_a < 10$.[50] Given that the ΔpK_a for [Mea][Ac] and [Mea][Hex] is ~4.75, the question about the proton transfer yields might arise. The proton transfer for amines and acetic acid was studied, and it was found out that, for primary amines, $\Delta pK_a > 4$ is enough to produce >99% ionization in this type of ionic liquids.[51] The exact extent of proton transfer in these systems, as well as the proton conduction mechanisms of interest for electrolyte applications (Grotthuss-like proton conduction), needs to be measured experimentally and through *ab initio* simulations to reach a conclusion.

There is a broad band from 2400 to 3700 cm^{-1}, known as the "the hydrogen stretching region", which results from the overlapping of the N−H, C−H, and O−H stretching modes of the amino alcohol with the O−H stretching modes of H_2O, which strongly absorbs in this region.[52] It is difficult to distinguish between the individual contributions, and as a consequence, the wavenumber region from 2400 to 4000 cm^{-1} did not provide useful information. However, a small signal of known origin can be seen at 3556 cm^{-1} when the ILs are mixed

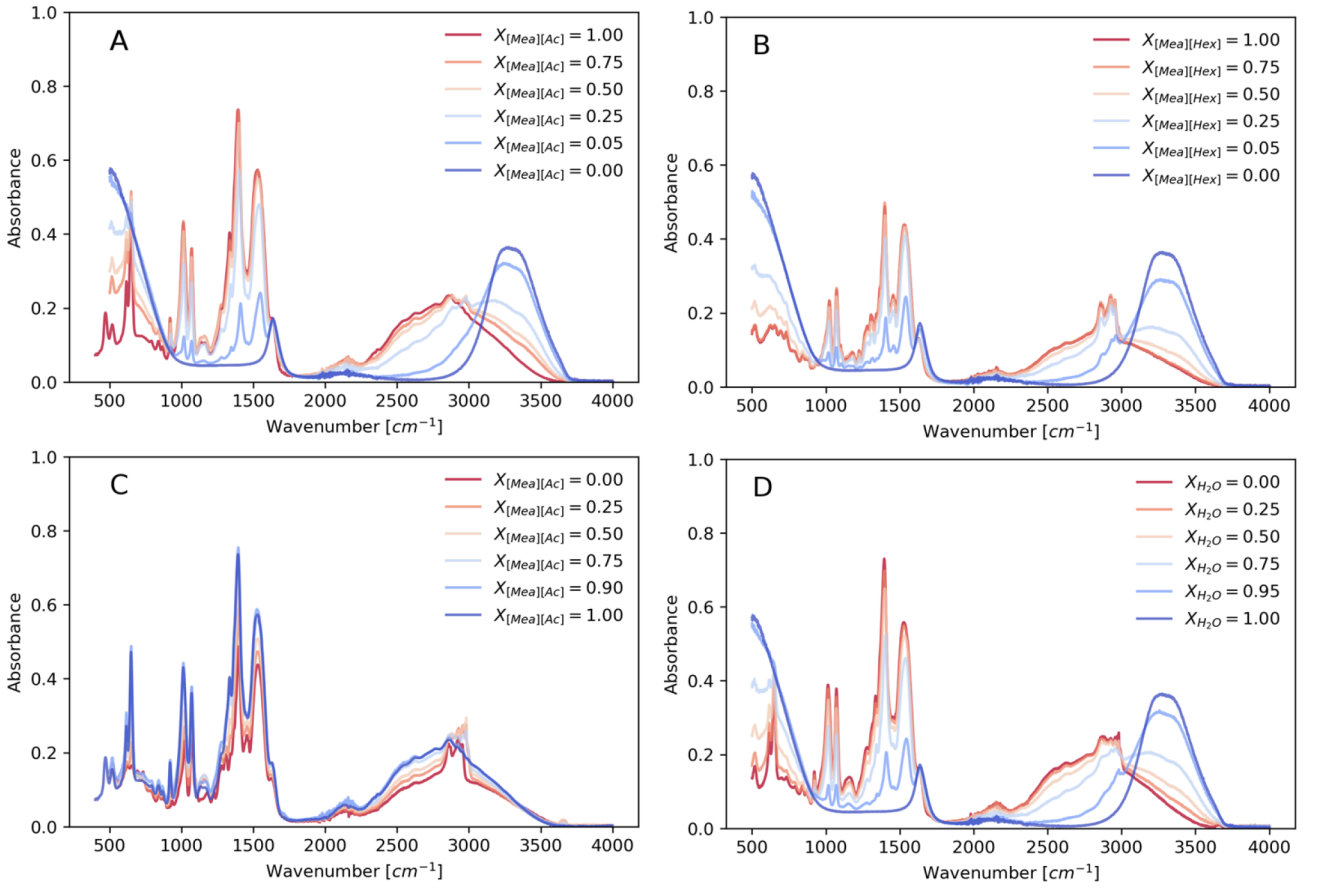

Figure 14. FTIR spectrum for different systems as a function of concentration in molar basis. (A) [Mea][Ac] and water mixtures. (B) [Mea][Hex] and water mixture. (C) Binary system: [Mea][Ac] and [Mea][Hex]. (D) Tertiary system: [Mea][Ac]:[Mea][Hex] (0.75:0.25 mole fraction) system diluted with water.

https://doi.org/10.1021/acs.jced.1c00687
J. Chem. Eng. Data 2022, 67, 1309−1325

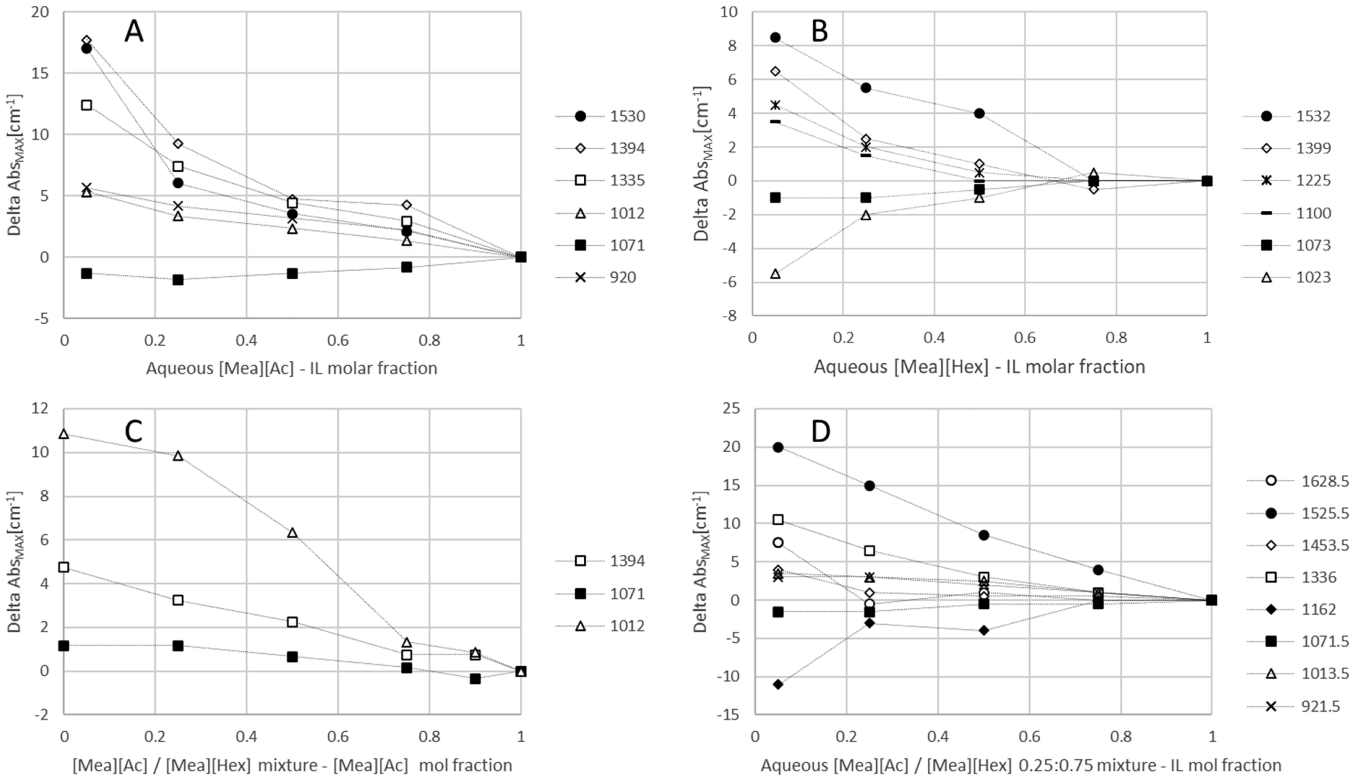

Figure 15. Water-induced shift for the binary mixture of ILs and water. (A) [Mea][Ac] and water mixtures. (B) [Mea][Hex] and water mixture. (C) Binary system: [Mea][Ac] and [Mea][Hex]. (D) Tertiary system: [Mea][Ac]:[Mea][Hex] (0.75:0.25 mol) system diluted with water.

in both aqueous and anhydrous conditions. For all diluted systems (x_{H_2O} = 0.95) (Figure 14A,B,D), a broad stretching band about 3350 cm^{-1} like the one of pure water can be seen, suggesting the presence of free water in these systems. At x_{H_2O} = 0.25 for the pure ILs, it can be seen from Figure 14A that the intensity of the FTIR absorption spectra in the 3350 cm^{-1} regions already differs from the anhydrous IL for [MEA][Ac], while no differences are seen for [MEA][Hex] (Figure 14B). This is consistent with the expected amount of water molecules to complete the hydration shells of these anions being smaller for the [Ac] anion than the [Hex] anion due to their molecular sizes. Therefore, a lesser number of water molecules are required to solvate the [Ac] anion, generating higher intensities in the 3350 cm^{-1} region of the FTIR spectra at the same molar faction compared to the [Hex] anion due to an increased number of water molecules beyond the first hydration shell. Advanced spectroscopic techniques and *ab initio* and molecular dynamic simulations are required to fully understand the hydrogen bonding network in these systems.

Upon water dilution of the neat ILs, as shown in Figure 13A,B, some signals experienced a water-induced shift. Figure 14 summarizes the magnitude of the water-induced shift of the absorption maximum as a function of IL/water concentration.

The wavenumber shifts observed upon dilution for [Mea][Ac] are as follows: 1530 cm^{-1} attributed to a combination of the symmetric rocking from the cation $\delta s(NH_3^+)$ and asymmetric stretching from the anion $\nu_{as}(COO^-)$, 1394 cm^{-1} $\nu_s(COO^-)$, 1335 cm^{-1} (CH_3 deformation, anion), 1071 cm^{-1} ν(C−N), 1012 cm^{-1} ν(C−OH), and 920 cm^{-1} (C−C stretching, anion). Those for [Mea][Hex] are as follows: 1532 cm^{-1} attributed to a combination of the symmetric rocking from the cation $\delta s(NH_3^+)$ and asymmetric stretching from the anion $\nu_{as}(COO^-)$, 1399 cm^{-1} $\nu_s(COO^-)$, 1225 cm^{-1} (CH_2 anion), 1100 cm^{-1} (CH_2 anion), 1071 cm^{-1} ν(C−N), and 1023 cm^{-1} ν(C−OH).

For both ILs, the signals involving (COO^-) vibration modes (~1530 and ~1394 cm^{-1}) experienced a water-induced blue shift, indicating that, with respect to the interactions involving this group and their direct environment in pure ILs, i.e., anion−cation, adding water induces a weakening of these interactions as a result of the higher affinity of the water molecules toward the carboxylic groups. A similar behavior has been observed for other [Ac]-based ILs.[53,54] In both systems, the ν(C−N) signal at 1071 cm^{-1} experienced a slight water-induced red shift. A similar phenomenon has been reported for imidazolium-based ILs, for which upon water dilution, there is a red shift of some vibrational modes of the cation concurrent with the strengthening of the hydrogen bond interaction with the proton acceptors.[54,55] An interesting result is the band attributed to the ν(C−OH) vibration, 1023 cm^{-1} for [Mea][Hex] and 1012 cm^{-1} for [Mea][Ac], which experienced a water-induced red shift for [Mea][Hex] and a blue shift in [Mea][Ac]. The blue shift is due to the weakening of the hydrogen bonding between the cation and anion due to the hydration of the carboxylic group in the [Ac] anion as previously discussed. The reason for the extreme red shift of the absorption band at 1023 cm^{-1} for [Mea]Hex] is not clear and should be further investigated with spectroscopic and computational methods. This strengthening upon dilution of that interactions between the cation−anion in [Mea][Hex] might be the cause of the density maxima shown in Figure 15.

The 1335 cm^{-1} signal attributed to the CH_3 deformation in the anion shows a water-induced blue shift in the case of the [Ac] anion, while this is not observed for the corresponding [Hex] moiety. This might be explained by the inability of the

https://doi.org/10.1021/acs.jced.1c00687
J. Chem. Eng. Data 2022, 67, 1309−1325

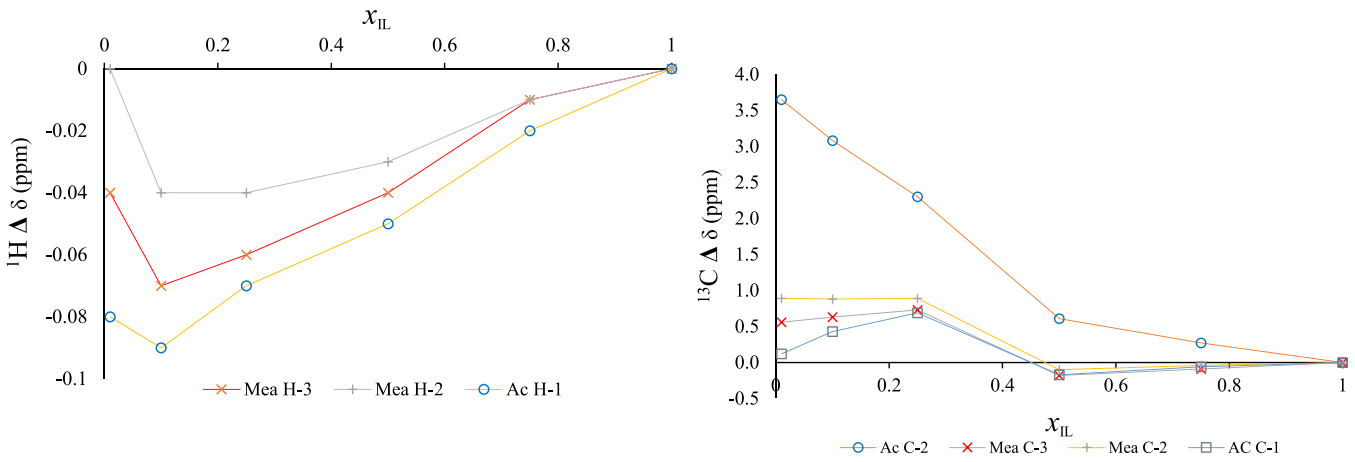

Figure 16. ^{1}H and ^{13}C delta chemical shifts for a [Mea][Ac] aqueous solution as a function of IL mole fraction.

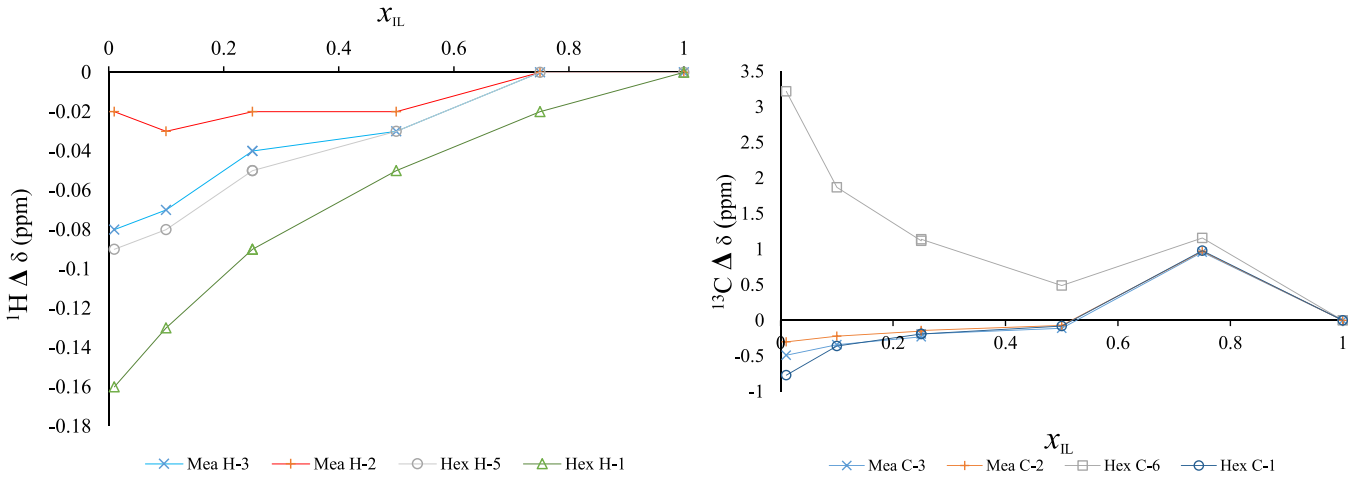

Figure 17. ^{1}H and ^{13}C delta chemical shifts for a [Mea][Hex] aqueous solution as a function of IL mol fraction.

[Ac] anions to aggregate to form micelles; therefore, the addition of water influences the chemical environment around the $-CH_3$. For the [Hex] anions in aqueous sodium of *n*-hexanoate, FTIR data have shown the formation of micelles that takes places in three stages. First, below ~0.75 M (x_{H2O} = 0.986), the solution is essentially monomeric. At a concentration of ~0.75 M, the onset of progressive aggregation can be seen with counterion binding. At a concentration of ~1.75 M (x_{H2O} = 0.963), there is a transition from a state of heterogeneous aggregation to a homogeneous micellar state.[56−58] By analogy, in the experiments performed in this study, all the [Hex] systems should be in a homogeneous micellar state as x_{H2O} < 0.963, which also corresponds to the region of maximum observed conductivity.

NMR. In terms of NMR spectroscopy, the straightforward variables that can be investigated are the chemical shifts of the signals in the ^{1}H and ^{13}C spectra. Secondary to the chemical shifts, both *T*1 and *T*2 relaxations reveal a lot of information about the physical composition of the sample.

The most obvious trend from this system is the change in both the intensity and the chemical shift in the water signal. In the most dilute system, the water signal appears at the expected 4.8 ppm. As the concentration of water is decreased, a downfield shift in the signal is observed in combination with a reduction in the signal. It should also be noted that the signal assigned to water is actually the average signal for all exchangeable protons from each species in solution. On decreasing the concentration of water, the relative contribution from these protons increases until the water concentration becomes negligible. While this result is not entirely surprising, the results of the change in the chemical shifts of the non-exchangeable protons are more remarkable.

While it is perhaps no revelation that a reduction in solvation due to waning water concentration may be expected to be linear or almost linear, a maximum change in chemical shift is observed in the region 0.10 to 0.25 M for [Mea][Ac], as depicted in Figure 16, which corresponds to the maxima for the V^E. In fact, this is most pronounced for the signals corresponding to protons 1 from acetate and 2 and 3 from ethanolamine (Figure 1). This overall upfield shift of the signals can be attributed to an overall net increase in hydrogen bonding and increase in structure resulting in a net increase in local electron density, especially for the signals attributed to ethanolamine that has both hydrogen bond acceptor and donor sites. As the water concentration is decreased, an overall loss of solvation due to hydrogen bonding causes a downfield shift in all peaks. Furthermore, there is also a steady increase in linewidth on decreasing water concentrations. A similar trend can be seen from the ^{13}C spectra assessment, as shown in Figure 16. Surprisingly, for the signals attributed to carbon 2 of acetate, an overall continued upfield shift is observed that would indicate an overall increase in electron density, possibly

https://doi.org/10.1021/acs.jced.1c00687
J. Chem. Eng. Data 2022, 67, 1309−1325

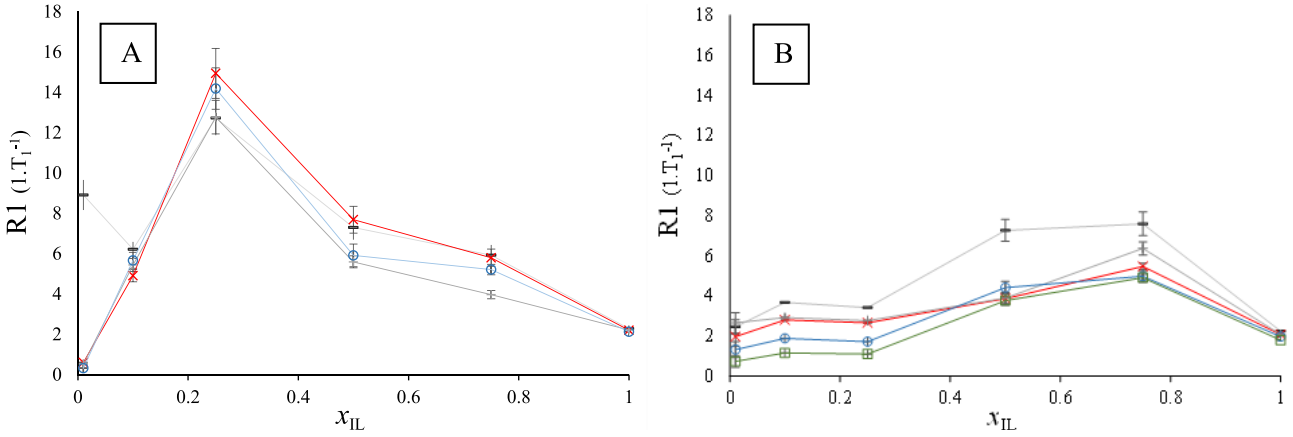

Figure 18. *R*1 relaxation for [Mea][Ac] and [Mea][Hex] as a function of IL mole fraction.

attributed to a loss in ionic character; this rate of change in chemical shift inflects at 50% mole fraction.

In contrast to the acetate system, the hexanoate ^{1}H δ signals do not show an overall maximum or minimum. An upfield shift at 0.75 mole fraction for protons 2 and 5 for hexanoate and 3 for ethanolamine and a constant upfield for proton 1 from hexanoate are observed, as depicted in Figure 17. The protons [Hex]-5 and [Mea]-3 seem to follow the same trend as water concentration increases, possibly due to water's close interaction to the charged sites from the IL, in accordance with what is observed for FTIR data. Likewise, for the acetate counterpart, line broadening is seen on increasing concentrations of ionic liquids. The signals for ^{13}C show a downfield maximum at 0.75 mole fraction ionic liquid followed by an overall upfield, as shown in Figure 17. The exception relies on [Hex]-6 carbon, which experiences a constant downfield after 0.5 IL mole fraction, as observed in [Ac]-1 carbon. This indicates the intense water interaction with the carboxylic site from both ILs, which is in accordance with the reported literature[2,19] and FTIR data.

Spin−lattice relaxation or longitudinal, more commonly reported as *T*1, relaxation may be described as the decay constant for the recovery of the magnetic moment toward equilibrium in the *Z* axis; this is typically measured by observing the decay in signal in the *XY* plane using inversion recovery experiments. Quantitatively, these results are reported as *R*1 $(1.T1^{-1})$.

The rates of R1 relaxation, as shown in Figure 18, of all signals also show a similar trend to the change in ^{1}H and ^{13}C chemical shifts. All relaxation rates reach a maximum at 0.25 IL mole fraction for [Mea][Ac], which can also be attributed to an increase in hydrogen bonding efficiency. The rates of longitudinal relaxation reach a maximum at around 0.75 [Mea][Hex] mole fraction, which also agrees with the ^{13}C data.

Transverse or spin−spin relaxation, more commonly reported as *T*2 relaxation, may be described as the loss of vector due to the dephasing of the spins and is qualitatively reported as *R*2 $(1.T2^{-1})$. The *R*2 relaxation rates were determined using the CPMG sequence.

As can be expected due to an overall decrease in mobility and subsequent increase in anisotropy, the *R*2 relaxation rates increase steadily. The increase in *R*2 relaxation rates concurs with the increased line widths observed for the proton signals. However, a close examination of the results reveals an inflection also in the range 0.10 to 0.25 IL (Figure S8). Similar to the acetate analogue, there is a net increase in spin−spin relaxation. However, it is clear from the trends that there is a sharper increase at 0.75 IL, which agrees with the other data.

The diffusion rates for each signal are summarized in Table S8 of the SI. As expected, an overall decrease in diffusion coefficients is seen on increasing the mole fraction of ionic liquids. There is, however, a steady region between 0.10 to 0.25 mole fraction [Mea][Ac]. This follows the same trends seen for changes in chemical shift and relaxation rates. For [Mea][Hex], a pronounced decrease in diffusion on increasing ionic liquid content is seen for the acetate counterpart. When comparing the diffusivities of the cation with respect to the anion for both ILs, [Mea] exhibits a close diffusion rate of that from acetate in the entire range of dilution. Conversely, in [Mea][Hex], the proximity is only observed above 0.75 IL mole fraction, suggesting that, for the latter, the cation mobility does not follow that of the anion [Hex] in the diluted regions under 0.75 IL mole fraction.

From the NMR assessment of the dry IL mixture, no significant trends are observed going from pure acetate to pure hexanoate in the anhydrous mixtures. This would indicate a stronger ionic binding for the more compact acetate system.

The IL proportion between [Ac] and [Hex] has a distinct effect on the diffusion rate depending on the water concentration. At the diluted region (0.75 water fraction), the acetate/hexanoate proportion, whether 0.25 or 0.75 mole fraction, has a negative effect on diffusion. Conversely, at concentrated regions (0.25 water fraction), the same proportions (0.25 and 0.75) have a positive effect on the species diffusion rate. [Ac] tends to diffuse faster than [Mea] and [Hex] as water concentration increases, with the lowest diffusion rate for the latter.

The calculated molar conductivity using the Nerst−Einstein equation ($\Lambda_{m,NE}$) was used to calculate the ionicity (I_{HR}) (equations in the SI). As per other ionic liquids and molten inorganic salts, the predicted conductivity for all systems calculated from self-diffusion data is higher than the experimental value ($\Lambda_{m,NE} > \Lambda$), resulting in an $I_{HR} < 1$ (results in the SI). This deviation of the measured conductivity from the Nernst−Einstein behavior is frequently interpreted by the formation of ion pairs or ion aggregates, which reduce the number of overall charge carriers.[59−62]

https://doi.org/10.1021/acs.jced.1c00687
J. Chem. Eng. Data 2022, 67, 1309−1325

CONCLUSIONS

Density and viscosity data of the neat ILs [Mea][Ac] and [Mea][Hex], the binary system (IL + water), and the tertiary system (IL mixture + water) have been measured in the range of 278.15 K (5 °C) to 363.15 K (90 °C) at the atmospheric pressure. Properties such as the molar volume, excess molar volume, and thermal expansion coefficient were also calculated. The observed V^E values were negative in the entire range of dilution and temperature for the binary and tertiary systems, considering both ILs.

[Mea][Ac]′ viscosity is more sensitive to temperature increase than [Mea][Hex], while their mixtures have a lower sensitivity than the neat ILs. The resulting viscosity of binary systems, for both [Mea][Ac] and [Mea][Hex] in water, were better predicted by the Herráez *et al.* model when considering an IL concentration above 0.25 mole fraction. Under this concentration, none of the used models exhibited an ADP inferior to 16%. For the binary systems [Mea][Ac] and [Mea][Hex], the lowest ADP (5.06%) was obtained using the Katti−Chaudhri model.

[Mea][Hex] has a lower surface tension than that observed for [Mea][Ac]. The presence of [Mea][Hex] leads to a reduction in the surface tension of [Mea][Ac] and water systems. Moreover, systems with [Mea][Hex] exhibited higher water activities than those from [Mea][Ac].

Although FTIR and NMR assessment suggests the occurrence of molecular events at 0.05, 0.25, 0.50, and 0.75 IL mole fractions, further investigation is required to elucidate the exact nature of such events.

ASSOCIATED CONTENT

Supporting Information

The Supporting Information is available free of charge at https://pubs.acs.org/doi/10.1021/acs.jced.1c00687.

Density and viscosity data of [Mea][Ac] and [Mea]-[Hex] mixtures in water at different temperatures (Table S1); predicted vs experimental density using eq Sq.2 (Table S3); conductivity of [Mea][Ac] and [Mea][Hex] solutions (Table S4); excess molar volumes of the [Mea][Hex]:[Mea][Ac] mixture (Figure S1); ln η versus variation in temperature (K) for the thermal expansion (α_p) determination (Figure S2); glass transition temperature of the studied systems (Table S5); DSC profiles of [Mea][Ac] and [Mea]Hex] mixtures (Figure S3); Arrhenius plot for IL classification in strong and fragile fluids (Figure S4); water adsorption and desorption profiles for [Mea][Ac], [Mea]Hex], and their equimolar mixture (Figure S5); surface tension for [Mea][Ac], [Mea]Hex], and their mixture in water (Table S6); ^{1}H and ^{13}C NMR of [Mea][Ac] (Figure S6); ^{1}H and ^{13}C NMR of [Mea][Hex] (Figure S7); ^{1}H spin−spin relaxation for [Mea][Ac] and [Mea][Hex] (Figure S8); 1H and 13C NMR chemical shifts for the binary systems IL:H_2O as a function of IL mole fraction (Table S7); diffusion rates of the studied components (Table S8); and ionicity and Nernst−Einstein molar conductivity (Table S9) (PDF)

AUTHOR INFORMATION

Corresponding Author

Forte Marcus Bruno − *Bioprocess and Metabolic Engineering Laboratory, Department of Food Engineering, Faculty of Food Engineering, University of Campinas (UNICAMP), São Paulo 13083-862, Brazil;* orcid.org/0000-0002-2263-4392; Email: forte@unicamp.br

Authors

Ferrari Felipe Augusto − *Bioprocess Engineering, Biotechnology Department, Faculty of Applied Sciences, Delft University of Technology (TUDelft), 2600 AA, Delft, The Netherlands; Bioprocess and Metabolic Engineering Laboratory, Department of Food Engineering, Faculty of Food Engineering, University of Campinas (UNICAMP), São Paulo 13083-862, Brazil*

Malaret Francisco − *Faculty of Engineering, Department of Chemical Engineering, Imperial College London, SW7 2AZ London, U.K.*

Eustace Stephen − *Biocatalysis, Biotechnology Department, Faculty of Applied Sciences, Delft University of Technology (TUDelft), 2600 AA, Delft, The Netherlands*

Hallett Jason − *Faculty of Engineering, Department of Chemical Engineering, Imperial College London, SW7 2AZ London, U.K.;* orcid.org/0000-0003-3431-2371

van der Wielen Luuk − *Bioprocess Engineering, Biotechnology Department, Faculty of Applied Sciences, Delft University of Technology (TUDelft), 2600 AA, Delft, The Netherlands*

Witkamp Geert-Jan − *Water Desalination and Reuse Center (WDRC), Division of Biological and Environmental Science and Engineering (BESE), King Abdullah University of Science and Technology (KAUST), Thuwal 23955-6900, Saudi Arabia*

Complete contact information is available at: https://pubs.acs.org/10.1021/acs.jced.1c00687

Notes

The authors declare no competing financial interest.

ACKNOWLEDGMENTS

Authors acknowledge the BE-Basic Foundation for financial support. F.A.F. acknowledges Max Zomerdijk, Yi Song, and Stef van Hateren of the Biotechnology Department at Applied Sciences (TUDelft) for technical support and Anton Firth of Imperial College for the productive discussions. The authors are grateful to Dr. Richard P. Matthews, Daphne Jackson Research Fellow of the Department of Chemical Engineering at Imperial College London, for the computational calculation of the FTIR spectra. F.A.F. and M.B.S.F. acknowledge FAPESP (2015/50612-8, 2017/24520-4, and 2019/19976-4) and the Biotechnology and Biological Sciences Research Council (BBSRC BB/P017460/1) for financial support. This work was conducted as part of a Dual Degree Ph.D. Project under the agreement between UNICAMP and TUDelft.

REFERENCES

(1) Koutsoukos, S.; Philippi, F.; Malaret, F.; Welton, T. A Review on Machine Learning Algorithms for the Ionic Liquid Chemical Space. *Chem. Sci.* **2021**, 6820.

(2) Nagi, D.; Thummuru, R.; Mallik, B. S. Structure and Dynamics of Hydroxyl-Functionalized Protic Ammonium Carboxylate Ionic Liquids. *J. Phys. Chem. A* **2017**, 8097−8107.

(3) Wang, B.; Qin, L.; Mu, T.; Xue, Z.; Gao, G. Are Ionic Liquids Chemically Stable? *Chem. Rev.* **2017**, *117*, 7113−7131.

(4) Stark, A. Ionic Liquids in the Biorefinery: A Critical Assessment of Their Potential. *Energy Environ. Sci.* **2011**, *4*, 19−32.

(5) Baaqel, H.; Díaz, I.; Tulus, V.; Chachuat, B.; Guillén-Gosálbez, G.; Hallett, J. P. Role of Life-Cycle Externalities in the Valuation of

Protic Ionic Liquids − a Case Study in Biomass Pretreatment Solvents. *Green Chem.* **2020**, 3132.
(6) Tzani, A.; Elmaloglou, M.; Kyriazis, C.; Aravopoulou, D.; Kleidas, I.; Papadopoulos, A.; Ioannou, E.; Kyritsis, A.; Voutsas, E.; Detsi, A. Synthesis and Structure-Properties Relationship Studies of Biodegradable Hydroxylammonium-Based Protic Ionic Liquids. *J. Mol. Liq.* **2016**, *224*, 366−376.
(7) Fumino, K.; Wulf, A.; Ludwig, R. The Potential Role of Hydrogen Bonding in Aprotic and Protic Ionic Liquids. *Phys. Chem. Chem. Phys.* **2009**, *11*, 8790−8794.
(8) Greaves, T. L.; Ha, K.; Muir, B. W.; Howard, S. C.; Weerawardena, A.; Kirby, N.; Drummond, C. J. Protic Ionic Liquids (PILs) Nanostructure and Physicochemical Properties: Development of High-Throughput Methodology for PIL Creation and Property Screens. *Phys. Chem. Chem. Phys.* **2015**, *17*, 2357−2365.
(9) Das, S. K.; Majhi, D.; Sahu, P. K.; Sarkar, M. Linking Diffusion−Viscosity Decoupling and Jump Dynamics in a Hydroxyl-Functionalized Ionic Liquid: Realization of Microheterogeneous Nature of the Medium. *ChemPhysChem* **2017**, *18*, 198−207.
(10) Deng, Y.; Husson, P.; Delort, A. M.; Besse-Hoggan, P.; Sancelme, M.; Costa Gomes, M. F. Influence of an Oxygen Functionalization on the Physicochemical Properties of Ionic Liquids: Density, Viscosity, and Carbon Dioxide Solubility as a Function of Temperature. *J. Chem. Eng. Data* **2011**, *56*, 4194−4202.
(11) Greaves, T. L.; Weerawardena, A.; Krodkiewska, I.; Drummond, C. J. Protic Ionic Liquids: Physicochemical Properties and Behavior as Amphiphile Self-Assembly Solvents. *J. Phys. Chem. B* **2008**, *112*, 896−905.
(12) Triolo, A.; Russina, O.; Bleif, H. J.; Di Cola, E. Nanoscale Segregation in Room Temperature Ionic Liquids. *J. Phys. Chem. B* **2007**, *111*, 4641−4644.
(13) Santos, D.; Lourenço, É.; Santos, M.; Santos, J. P.; Franceschi, E.; Barison, A.; Mattedi, S. Properties of Aqueous Solutions of Ammonium-Based Ionic Liquids and Thermodynamic Modelling Using Flory Theory. *J. Mol. Liq.* **2017**, *229*, 508−513.
(14) Chhotaray, P. K.; Gardas, R. L. Thermophysical Properties of Ammonium and Hydroxylammonium Protic Ionic Liquids. *J. Chem. Thermodyn.* **2014**, *72*, 117−124.
(15) Pin, T. C.; Nakasu, P. Y. S.; Mattedi, S.; Rabelo, S. C.; Costa, A. C. Screening of Protic Ionic Liquids for Sugarcane Bagasse Pretreatment. *Fuel* **2019**, *235*, 1506−1514.
(16) Dias, R. M.; da Costa Lopes, A. M.; Silvestre, A. J. D.; Coutinho, J. A. P.; da Costa, M. C. Uncovering the Potentialities of Protic Ionic Liquids Based on Alkanolammonium and Carboxylate Ions and Their Aqueous Solutions as Non-Derivatizing Solvents of Kraft Lignin. *Ind. Crops Prod.* **2020**, *143*, 111866.
(17) Nakasu, P. Y. S.; Ienczak, J. L.; Rabelo, S. C.; Costa, A. C. The Water Consumption of Sugarcane Bagasse Post-Washing after Protic Ionic Liquid Pretreatment and Its Impact on 2G Ethanol Production. *Ind. Crops Prod.* **2021**, *169*, 113642.
(18) Alvarez, V. H.; Mattedi, S.; Martin-Pastor, M.; Aznar, M.; Iglesias, M. Thermophysical Properties of Binary Mixtures of {ionic Liquid 2-Hydroxy Ethylammonium Acetate + (Water, Methanol, or Ethanol)}. *J. Chem. Thermodyn.* **2011**, *43*, 997−1010.
(19) Hosseini, S. M.; Hosseinian, A.; Aparicio, S. An Experimental and Theoretical Study on 2-Hydroxyethylammonium Acetate Ionic Liquid. *J. Mol. Liq.* **2019**, *284*, 271−281.
(20) Villar-Garcia, I. J.; Lovelock, K. R. J.; Men, S.; Licence, P. Tuning the Electronic Environment of Cations and Anions Using Ionic Liquid Mixtures. *Chem. Sci.* **2014**, *5*, 2573−2579.
(21) Xiao, Y.; Huang, X. The Physicochemical Properties of a Room-Temperature Liquidus Binary Ionic Liquid Mixture of [HNMP][CH3SO3]/[Bmim]Cl and Its Application for Fructose Conversion to 5-Hydroxymethylfurfural. *RSC Adv.* **2018**, *8*, 18784−18791.
(22) Ferrari, F. A.; Pereira, J. F. B.; Witkamp, G. J.; Forte, M. B. S. Which Variables Matter for Process Design and Scale-up? A Study of Sugar Cane Straw Pretreatment Using Low-Cost and Easily Synthesizable Ionic Liquids. *ACS Sustainable Chem. Eng.* **2019**, *7*, 12779−12788.
(23) Ferrari, F. A. *Processing Lignocellulosic Feedstock Using Ionic Liquids for Biorefinery Application*; Delft University of Technology, 2021.
(24) Chirico, R. D.; Frenkel, M.; Magee, J. W.; Diky, V.; Muzny, C. D.; Kazakov, A. F.; Kroenlein, K.; Abdulagatov, I.; Hardin, G. R.; Acree, W. E.; Brenneke, J. F.; Brown, P. L.; Cummings, P. T.; De Loos, T. W.; Friend, D. G.; Goodwin, A. R. H.; Hansen, L. D.; Haynes, W. M.; Koga, N.; Mandelis, A.; Marsh, K. N.; Mathias, P. M.; McCabe, C.; O'Connell, J. P.; Pádua, A.; Rives, V.; Schick, C.; Trusler, J. P. M.; Vyazovkin, S.; Weir, R. D.; Wu, J. Improvement of Quality in Publication of Experimental Thermophysical Property Data: Challenges, Assessment Tools, Global Implementation, and Online Support. *J. Chem. Eng. Data* **2013**, *58*, 2699−2716.
(25) Usula, M.; Plechkova, N. V.; Piras, A.; Porcedda, S. Ethylammonium Alkanoate-Based Ionic Liquid + Water Mixtures. *J. Therm. Anal. Calorim.* **2015**, *121*, 1129−1137.
(26) Hosseini, S. M.; Alavianmehr, M. M.; Gutiérrez, A.; Khalifeh, R.; Moghadasi, J.; Aparicio, S. On the Properties and Structure of 2-Hydroxyethylammonium Formate Ionic Liquid. *J. Mol. Liq.* **2018**, *249*, 233−244.
(27) Sarabando, J. A.; Magano, P. J. M.; Ferreira, A. G. M.; Santos, J. B.; Carvalho, P. J.; Mattedi, S.; Fonseca, I. M. A. Influence of Temperature and Pressure on the Density and Speed of Sound of 2-Hydroxyethylammonium Propionate Ionic Liquid. *J. Chem. Thermodyn.* **2018**, *122*, 183−193.
(28) Yunus, N. M.; Halim, N. H.; Wilfred, C. D.; Murugesan, T.; Lim, J. W.; Show, P. L. Thermophysical Properties and CO2 Absorption of Ammonium-Based Protic Ionic Liquids Containing Acetate and Butyrate Anions. *Processes* **2019**, *7*, 820.
(29) Rocha Pinto, R.; Santos, D.; Mattedi, S.; Aznar, M. Density, refractive index, apparent volumes and excess molar volumes of four protic ionic liquids+ water at T= 298.15 and 323.15 K. *Braz. J. Chem. Eng.* **2015**, *32*, 671−682.
(30) Sánchez, P. B.; García, J.; Pádua, A. A. H. Structural Effects on Dynamic and Energetic Properties of Mixtures of Ionic Liquids and Water. *J. Mol. Liq.* **2017**, *242*, 204−212.
(31) Shi, J.; Balamurugan, K.; Parthasarathi, R.; Sathitsuksanoh, N.; Zhang, S.; Stavila, V.; Subramanian, V.; Simmons, B. A.; Singh, S. Understanding the Role of Water during Ionic Liquid Pretreatment of Lignocellulose: Co-Solvent or Anti-Solvent? *Green Chem.* **2014**, *16*, 3830−3840.
(32) Glasser, L.; Jenkins, H. D. B. Predictive Thermodynamics for Ionic Solids and Liquids. *Phys. Chem. Chem. Phys.* **2016**, *18*, 21226−21240.
(33) Latawiec, A. E.; Strassburg, B. B. N.; Valentim, J. F.; Ramos, F.; Alves-Pinto, H. N. Intensification of Cattle Ranching Production Systems: Socioeconomic and Environmental Synergies and Risks in Brazil. *Animal* **2014**, *8*, 1255−1263.
(34) Chennuri, B. K.; Gardas, R. L. Measurement and Correlation for the Thermophysical Properties of Hydroxyethyl Ammonium Based Protic Ionic Liquids: Effect of Temperature and Alkyl Chain Length on Anion. *Fluid Phase Equilib.* **2016**, *427*, 282−290.
(35) Vila, J.; Ginés, P.; Pico, J. M.; Franjo, C.; Jiménez, E.; Varela, L. M.; Cabeza, O. Temperature Dependence of the Electrical Conductivity in EMIM-Based Ionic Liquids: Evidence of Vogel-Tamman-Fulcher Behavior. *Fluid Phase Equilib.* **2006**, *242*, 141−146.
(36) Metatla, N.; Soldera, A. The Vogel-Fulcher-Tamman Equation Investigated by Atomistic Simulation with Regard to the Adam-Gibbs Model. *Macromolecules* **2007**, *40*, 9680−9685.
(37) Grunberg, L.; Nissan, A. Mixture Law for Viscosity. *Nature* **1949**, *164*, 799−800.
(38) Kendall, J.; Monroe, K. P. The viscosity of liquids. II. The viscosity-composition curve for ideal liquid mixtures. *J. Am. Chem. Soc.* **1917**, *39*, 1787−1802.
(39) Frenkel, Y. I. *Kinetic Theory of Liquids*; Dover: New York, 1955.
(40) Eyring, H. Examples of Absolute Reaction Rates. *J. Chem. Phys.* **1936**, *283* ().

https://doi.org/10.1021/acs.jced.1c00687
J. Chem. Eng. Data 2022, 67, 1309−1325

(41) Adam, O. E. A. A.; Awwad, A. M. Estimation of Excess Molar Volumes and Theoretical Viscosities of Binary Mixtures of Benzene + N-Alkanes at 298.15 K. *Int. J. Ind. Chem.* **2016**, *7*, 391−400.
(42) Katti, P. K.; Chaudhri, M. M. Viscosities of Binary Mixtures of Benzyl Acetatewith Dioxane, Aniline, and m-Cresol. *J. Chem. Eng. Data* **1964**, *9*, 442−443.
(43) Herráez, J. V.; Belda, R.; Díez, O.; Herráez, M. An Equation for the Correlation of Viscosities of Binary Mixtures. *J. Solution Chem.* **2008**, *37*, 233−248.
(44) Van Der Wielen, L. A. M.; Zomerdijk, M.; Houwers, J.; Luyben, K. C. A. M. Diffusivities of Organic Electrolytes in Water. *Chem. Eng. J.* **1997**, *66*, 111−121.
(45) Watanabe, H.; Umecky, T.; Arai, N.; Nazet, A.; Takamuku, T.; Harris, K. R.; Kameda, Y.; Buchner, R.; Umebayashi, Y. Possible Proton Conduction Mechanism in Pseudo-Protic Ionic Liquids: A Concept of Specific Proton Conduction. *J. Phys. Chem. B* **2019**, *123*, 6244−6252.
(46) Xu, W.; Wang, L. M.; Nieman, R. A.; Angell, C. A. Ionic Liquids of Chelated Orthoborates as Model Ionic Glassformers. *J. Phys. Chem. B* **2003**, *107*, 11749−11756.
(47) Greaves, T. L.; Weerawardena, A.; Fong, C.; Krodkiewska, I.; Drummond, C. J. Protic Ionic Liquids: Solvents with Tunable Phase Behavior and Physicochemical Properties. *J. Phys. Chem. B* **2006**, *110*, 22479−22487.
(48) Brooks, N. J.; Castiglione, F.; Doherty, C. M.; Dolan, A.; Hill, A. J.; Hunt, P. A.; Matthews, R. P.; Mauri, M.; Mele, A.; Simonutti, R.; Villar-Garcia, I. J.; Weber, C. C.; Welton, T. Linking the Structures, Free Volumes, and Properties of Ionic Liquid Mixtures. *Chem. Sci.* **2017**, *8*, 6359−6374.
(49) Angell, C. A. The Old Problems of Glass and the Glass Transition, and the Many New Twists. *Proc. Natl. Acad. Sci.* **1995**, *92*, 6675−6682.
(50) Belieres, J.-P.; Angell, C. A. Protic Ionic Liquids: Preparation, Characterization, and Proton Free Energy Level Representation †. *J. Phys. Chem. B* **2007**, *111*, 4926−4937.
(51) Stoimenovski, J.; Izgorodina, E. I.; MacFarlane, D. R. Ionicity and Proton Transfer in Protic Ionic Liquids. *Phys. Chem. Chem. Phys.* **2010**, *12*, 10341.
(52) Richner, G.; Puxty, G. Assessing the Chemical Speciation during CO 2 Absorption by Aqueous Amines Using in Situ FTIR. *Ind. Eng. Chem. Res.* **2012**, *51*, 14317−14324.
(53) Marekha, B. A.; Bria, M.; Moreau, M.; De Waele, I.; Miannay, F.-A.; Smortsova, Y.; Takamuku, T.; Kalugin, O. N.; Kiselev, M.; Idrissi, A. Intermolecular Interactions in Mixtures of 1-n-Butyl-3-Methylimidazolium Acetate and Water: Insights from IR, Raman, NMR Spectroscopy and Quantum Chemistry Calculations. *J. Mol. Liq.* **2015**, *210*, 227−237.
(54) Chen, Y.; Cao, Y.; Zhang, Y.; Mu, T. Hydrogen Bonding between Acetate-Based Ionic Liquids and Water: Three Types of IR Absorption Peaks and NMR Chemical Shifts Change upon Dilution. *J. Mol. Struct.* **2014**, *1058*, 244−251.
(55) Cha, S.; Ao, M.; Sung, W.; Moon, B.; Ahlström, B.; Johansson, P.; Ouchi, Y.; Kim, D. Structures of Ionic Liquid−Water Mixtures Investigated by IR and NMR Spectroscopy. *Phys. Chem. Chem. Phys.* **2014**, *16*, 9591−9601.
(56) Umemura, J.; Cameron, D. G.; Mantsch, H. H. An FT-IR Study of Micelle Formation in Aqueous Sodium n-Hexanoate Solutions. *J. Phys. Chem.* **1980**, 2272.
(57) Campbell, A. N.; Friesen, J. I. CONDUCTANCES OF AQUEOUS SOLUTIONS OF SODIUM HEXANOATE (SODIUM CAPROATE) AND THE LIMITING CONDUCTANCES OF THE HEXANOATE ION, AT 25 °C AND 35 °C. *Can. J. Chem.* **1960**, 1939.
(58) Umemura, J.; Mantsch, H. H.; Cameron, D. G. Micelle Formation in Aqueous N-Alkanoate Solutions: A Fourier Transform Infrared Study. *J. Colloid Interface Sci.* **1981**, 558.
(59) Ueno, K.; Tokuda, H.; Watanabe, M. Ionicity in Ionic Liquids: Correlation with Ionic Structure and Physicochemical Properties. *Phys. Chem. Chem. Phys.* **2010**, *12*, 1649.
(60) Rüther, T.; Kanakubo, M.; Best, A. S.; Harris, K. R. The Importance of Transport Property Studies for Battery Electrolytes: Revisiting the Transport Properties of Lithium−N-Methyl-N-Propylpyrrolidinium Bis(Fluorosulfonyl)Imide Mixtures. *Phys. Chem. Chem. Phys.* **2017**, *19*, 10527−10542.
(61) Schmidt, J. R.; Skinner, J. L. Hydrodynamic Boundary Conditions, the Stokes−Einstein Law, and Long-Time Tails in the Brownian Limit. *J. Chem. Phys.* **2003**, *119*, 8062−8068.
(62) Rauber, D.; Hofmann, A.; Philippi, F.; Kay, C. W. M.; Zinkevich, T.; Hanemann, T.; Hempelmann, R. Structure-Property Relation of Trimethyl Ammonium Ionic Liquids for Battery Applications. *Appl. Sci.* **2021**, *11*, 5679.

https://doi.org/10.1021/acs.jced.1c00687
J. Chem. Eng. Data 2022, 67, 1309−1325